THE ASTRONOMICAL JOURNAL, 121:1974–1991, 2001 April

AGES AND METALLICITIES OF FORNAX DWARF ELLIPTICAL GALAXIES

KARL RAKOS
Institute for Astronomy, University of Vienna, A-1180, Wien, Austria; karl.rakos@chello.at
JAMES SCHOMBERT
Department of Physics, University of Oregon, Eugene, OR 97403; js@abyss.uoregon.edu
H. M. MAITZEN
Institute for Astronomy, University of Vienna, A-1180, Wien, Austria
SINISA PRUGOVECKI
University of Zagreb, Croatia
AND
ANDREW ODELL
Department of Physics and Astronomy, Box 6010, Northern Arizona University, Flagstaff, AZ 86011; andy.odell@nau.edu
Received 2000 October 16; accepted 2000 December 28

ABSTRACT

Narrowband photometry is presented on 27 dwarf ellipticals in the Fornax cluster. Calibrated with Galactic globular cluster data and spectrophotometric population models, the colors indicated that dwarf ellipticals have a mean [Fe/H] of -1.00 ± 0.28 ranging from -1.6 to -0.4. The mean age of dwarf ellipticals, also determined photometrically, is estimated at 10 ± 1 Gyr compared with 13 Gyr for bright Fornax ellipticals. Comparison of our metallicity color and Mg_2 indices demonstrates that the [Mg/Fe] ratio is lower in dwarf ellipticals than their more massive cousins, which is consistent with a longer duration of initial star formation to explain their younger ages. There is a increase in dwarf metallicity with distance from the Fornax cluster center, where core galaxies are on average 0.5 dex more metal-poor than halo dwarfs. In addition, we find the halo dwarfs are younger in mean age compared with core dwarfs. One possible explanation is that the intracluster medium ram pressure strips the gas from dwarf ellipticals, halting star formation (old age) and stopping enrichment (low metallicity) as they enter the core.

Key words: galaxies: dwarf — galaxies: elliptical and lenticular, cD — galaxies: evolution — galaxies: stellar content

1. INTRODUCTION

Objects composed of single stellar populations (SSP, i.e., globular clusters) or a composite of SSPs (i.e., ellipticals) present special circumstances for the study of the evolution of stellar populations. A SSP is a stellar population of instantaneous origin at a particular formation time with a single metallicity. For many galaxies, the resolution of the integrated population into a series of composite SSPs is impossible because of the presence of ongoing star formation. However, for systems that have exhausted their gas supply many gigayears ago, it may be possible to untangle the underlying population with some simple assumptions. The canonical interpretation of the spectroscopy and photometric data for ellipticals is that they are a composite of a series of SSPs with a small spread in age that represents the time from the initial burst of star formation (Charlot & Bruzual 1991), although there is new data to indicate that a significant number of field ellipticals have a large spread in age (see Trager et al. 2000). Because of the fact that the initial star formation occurs over some finite duration (i.e., not simultaneous), enrichment of the ISM by supernovae and stellar winds will alter the successive generation of stars, producing a smooth increase in mean metallicity.

Only recently have we achieved evolution models with the proper input physics and stellar libraries of metal-poor to super–metal-rich stars, which can follow the photometric changes due to enrichment from previous populations (e.g., Bruzual & Charlot 2001, hereafter BC2001). The two most prominent observables to the effects of population evolution in ellipticals are the mass-metallicity effect, the higher mean metallicity for high-mass galaxies, and the existence of metallicity gradients. The very existence of metallicity gradients demonstrates that some process of chemical evolution occurs since a gradient develops by the freezing of the metallicity as a function of time in the orbits of the first generation stars (i.e., oldest and metal-poor) at the outer radii and most enriched in the core.

Any investigation into the stellar populations in ellipticals must focus on the separation of the age and metallicity to the underlying stars as the two key parameters. Unfortunately, slight changes in age and metallicity operate in the same direction of spectroevolutionary parameter space, the well-known age-metallicity degeneracy. Recently, the age-metallicity degeneracy has been broken with the use of spectral line indices (Worthey 1994), but the problem of light element enrichment plagues the interpretation of line results (Worthey 1998). While spectral indices are usually considered superior to colors in the determination of age and metallicity factors, narrowband colors have a distinct advantage when the expected age differences will be small and, thus, higher S/N of the kind offered by integrated color will be required for any spatial coverage. In addition, many of the best line indices (H and K Ca, Mg_2) suffer from subtle effects (e.g., α enhancement to nonsolar values) that make interpretation of age and metallicity model dependent.

Most of what we have determined about the stellar populations in ellipticals has centered on high-mass, bright ellipticals while their lesser cousins, the dwarf ellipticals, have

received little attention. Dwarf ellipticals are, by definition, low in apparent magnitude and the primary difficulty in obtaining information about their stellar populations is because their surface brightnesses are very low making spectral observations difficult regardless of distance. This is unfortunate because dwarf galaxies are important to our understanding of galaxy formation and evolution. For example, hierarchical models of structure formation hypothesize that all galaxies are constructed from the merger of smaller mass dwarfs. Even with their low surface brightnesses, there is no shortage in the number of dwarf ellipticals to study since they make up a significant fraction of the members of rich clusters (Ferguson & Binggeli 1994). There have been numerous studies of the properties of dwarfs (e.g., Bothun et al. 1986); however, there is no solid consensus on the interpretation of the stellar content of dwarfs. For example, in an experiment applied by Arimoto (1996), the spectral templates of dwarf ellipticals was distributed to numerous population synthesis groups. The results concluded that dwarf ellipticals were either (1) old and metal-rich, (2) old and slightly metal-poor ([Fe/H] ≈ -0.3), or (3) young (3–5 Gyr) and solar metallicity.

For the last 15 years, our group has used a narrowband filter system to explore the color evolution of galaxies in distant clusters. This filter system, a modified Strömgren color system, was used initially to follow the color evolution of ellipticals to a redshift of 0.9 (Rakos & Schombert 1995). However, the Strömgren colors were also found to be a sharp discriminator of star-forming galaxies in clusters (the Butcher-Oemler effect) and, most importantly, several of the indices were found to have good correlations with metallicity in a study of color gradients in ellipticals (Schombert et al. 1993). The color system displayed promise as an avenue to investigate the properties of SSPs without the need for extensive model interpretation.

Our goal for this paper is twofold: (1) to demonstrate that narrowband filters are effective in discriminating age and metallicity for single-generation objects and (2) to use our narrowband system to compare the stellar populations in dwarf and giant ellipticals. While spectral indices are superior in the detailed information they provide, our goal is to develop a system that can be used for low surface brightness and/or distant objects, where spectroscopy is impractical.

Because of the need to connect our filter system to the Galactic globular cluster age and metallicity system, as well as demonstrate the effects of multimetallicity SSPs on the integrated colors of ellipticals, the presentation of the data is lengthy. However, we have divided the paper into the following topics, comparison with globular clusters, comparison with SSP models, empirical age and metallicity calibration and discussion of the properties of dwarfs compared with bright ellipticals, in order to allow the reader to focus on the sections of their interest. Most of our results are model independent; however, we have made every effort to single out the observationally secure conclusions from the ones requiring theoretical assistance.

2. OBSERVATIONS

2.1. *Strömgren Filter System*

The data for this project were collected using a modified Strömgren filter system. The original Strömgren *uvby* filter system and its extensions (Strömgren 1966; Wood 1969) were developed to provide the astronomical community with an accurate means of measuring the temperature, chemical composition and surface gravity of stars, without resorting to high-resolution spectroscopy. This is achieved by selecting center wavelengths to cover regions of the stellar spectral energy distributions (SED) which are sensitive to the above properties. This provided an efficient and quantifiable method of sampling stellar types without the use of qualitative spectral classification (e.g., the MK scheme).

In the late 1980s, our team developed a modified Strömgren system (called *uz*, *vz*, *bz*, *yz*), which was a rest-frame narrowband filter system used primarily to investigate the spectrophotometric evolution of distant galaxies. While similar to the *uvby* system, the *uz*, *vz*, *bz*, *yz* filters are slightly narrower and the filter response curves are more symmetrically shaped then the original filters. The *uz*, *vz*, *bz*, *yz* system covers three regions in the near-UV and blue portion of the spectrum that make it a powerful tool for the investigation of stellar populations in SSPs, such as star clusters, or composite systems, such as galaxies. The first region is longward of 4600 Å, where in the influence of absorption lines is small. This is characteristic of the *bz* and *yz* filters ($\lambda_{\rm eff} = 4675$ and 5500 Å), which produce a temperature color index, $bz-yz$. The second region is a band shortward of 4600 Å, but above the Balmer discontinuity. This region is strongly influenced by metal absorption lines (i.e., Fe, CN) particularly for spectral classes F to M, which dominate the contribution of light in old stellar populations. This region is exploited by the *vz* filter ($\lambda_{\rm eff} =$ 4100 Å). The third region is a band shortward of the Balmer discontinuity or below the effective limit of crowding of the Balmer absorption lines. This region is explored by the *uz* filter ($\lambda_{\rm eff} = 3500$ Å). All the filters are sufficiently narrow (FWHM = 200 Å) to sample regions of the spectrum unique to the various physical processes of star formation and metallicity.

Originally, the *uz*, *vz*, *bz*, *yz* system was convolved with model atmospheres and Galactic standards to determine its behavior as a function of stellar type and metallicity. Later, comparison with stellar population models (Arimoto & Yoshii 1986; Guiderdoni & Rocca-Volmerange 1987; BC2001) was used to set the zero points for our color system. All SED models are presented as a set of spectral energy distributions listing flux (ergs per square centimeter per second per angstrom) as a function of wavelength. Our *uz*, *vz*, *by*, *yz* colors are determined by convolving the SEDs to our filter sensitivity curves (Rakos & Schombert 1995). As an example, two SED models of $Z = 0.0001$ and $Z = 0.02$ (where solar [Fe/H] corresponds to $Z = 0.02$) and our filter bandpasses are shown in Figure 1 for a SSP of age 13 Gyr (the SEDs have been normalized at 5500 Å). The known trend of bluer colors for the metal-poor populations is obvious. Note also that the bluer population for the metal-poor model changes the general shape of the SED and that the increase in the strength of metal absorption features sharpens the 4000 Å break in the metal-rich model. This is an important point since any interpretation of a color system requires calibration of the effects of line blanketing, as well as the changes in the effective temperature of the stellar population. In addition, the effects of luminosity weighted fluxes from different metallicity populations will produce significant changes in the integrated colors (see § 2.3).

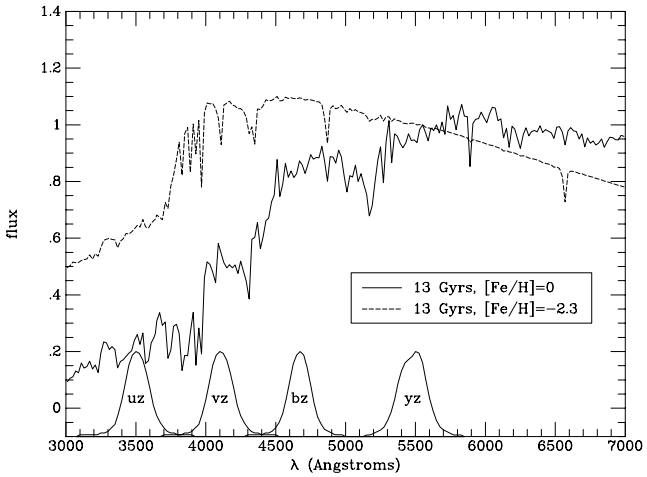

FIG. 1.—SSP models from BC2001. The models for a 13 Gyr metal-poor and a 13 Gyr metal-rich population are shown normalized to the 5500 Å flux. The filter response curves for *uz*, *vz*, *bz*, and *yz* are shown. The effects of increased line blanketing and cooler mean temperatures are evident in the stronger spectral features, and they shift with the peak luminosity to longer wavelengths.

The Guiderdoni & Rocca-Volmerange models were used to trace the color evolution of ellipticals out to redshifts of 0.9 (Rakos & Schombert 1995), and the analysis was a good example of the interplay between models and observations. For example, the data on ellipticals indicated a red "bump" at redshifts of 0.4. This bump is visible in both the continuum $bz-yz$ and metallicity $vz-yz$ indices. The Guiderdoni & Rocca-Volmerange models, which incorporated the details of the late stages of stellar evolution (HB and AGB populations), predicted this color bump as due to a 8 Gyr old HB contribution that peaked at that particular epoch (on the assumption of a galaxy formation epoch at a redshift of 5). However, the metallicity colors ($vz-yz$) for the bump and more distant clusters were bluer than Guiderdoni & Rocca-Volmerange model predictions. That difference was due to the lack of a variation in metallicity in the stellar templates used to produce the SED models. The models of Arimoto & Yoshii corrected this deficiency and predicted the bluer $vz-yz$ colors in a burst population. The integrated light from present-day ellipticals is primarily from red giant branch (RGB) and turnoff main sequence stars (TO), but in the past (even as recent as 4 Gyr ago) the contribution from metal-poor HB and AGB stars increases to a noticeable fraction of the total light. Thus, the color evolution of ellipticals demonstrated the need for models which not only contained the details of the late stages of stellar evolution plus also incorporated a full treatment of chemical evolution that follows the extended burst of star formation that created the first generations.

The *uz*, *vz*, *bz*, *yz* system is designed to match the rest frames of distant clusters so as to minimize *k*-corrections. However, in a parallel study to the distant ellipticals, the zero-redshift filters were applied to a set of nearby, bright ellipticals to search for color gradients (Schombert et al. 1993). Color gradients reflect either age or metallicity changes during the formation of a galaxy. Current studies strongly indicate that gradients are primarily metallicity induced (Kodama & Arimoto 1997), but the Schombert et al. data suggested a problem in the *uz*, *vz*, *bz*, *yz* system calibration to Mg_2 due to possible light element abundance enhancement in ellipticals (Worthey 1998). To investigate this possibility, we have undertaken a program to relink the *uz*, *vz*, *bz*, *yz* system to the metallicity of globular clusters, particularly since a study of low-mass galaxies will enter the realm of less than solar metallicities that few models have attempted.

2.2. *Globular Clusters*

In order to relink the *uz*, *vz*, *bz*, *yz* system to the metallicity system defined by globular clusters, a series of metal-rich and metal-poor systems were observed between 1997 and 1999 from both the Northern and Southern Hemisphere. The northern cluster observations were made at Lowell Observatory using 1.1 m Hall telescope. The imaging device was the SIT 2K CCD with 24 μm pixels binned 4 × 4. The field size covers 18′ × 18′ of sky. The southern cluster observations were made at CTIO using the 0.91 m Curtis Schmidt telescope plus STIS 2K CCD with 21 μm pixels. The plate scale of 2.″1 pixel^{-1} covers 76′ × 76′ of sky. Reduction followed standard CCD procedures (bias, flat field, etc.). Standard spectrophotometric stars were used for calibrations following the same procedures for our distant galaxy program (see Fiala, Rakos, & Stockton 1986; Rakos, Fiala, & Schombert 1988). Reddenings were calculated according to Rakos, Maindl, & Schombert (1996), taking into account the $E(B-V)$ values from the literature and compiled by Harris (1996). One of the primary goals of the project is to calibrate an age and metallicity relation from the SSPs in globular clusters. To this end, we have placed a special emphasis on selecting a set of clusters with varying [Fe/H] and age values. Since age and metallicity are correlated in our own Galaxy, it was not possible to completely fill the parameter space of the two. However, we have attempted to observe a maximum range in metallicities in halo and disk clusters of similar age.

Since our primary interest is the integrated color of main stellar population that comprises the globular clusters, special attention was given to the influence of foreground stars (due to low Galactic latitude for most of the sample) and to possible color changes with the aperture radius. To investigate the aperture effect, plots were made of the various colors ($uz-vz$, $vz-yz$, and $bz-yz$) as a function of aperture radius. One example is shown in Figure 2 for cluster NGC 6723 ($b = -17°$). Very little change in color is found outside the inner 40″ of the cluster (the half light radius for cluster is 85″). This confirms previous work that there is little change in the stellar population of a globular cluster from core to edge in terms of mean color of the stars. Experimentation demonstrated that the most stable aperture is the half-light radius of the cluster.

The influence of the foreground stars is estimated by measuring several regions on each CCD frame outside of the cluster. The total difference between cluster and brightness in the neighborhood was, on average, at least 5 mag fainter (for the same aperture size) than the cluster luminosity. This would account for at most 0.010 mag of total light. Experimentation with sky subtraction produced a variance of only 0.005 mag in cluster color at the half-light radius. The accuracy of our final measurements ranged from 0.005 to 0.015 mag depending on the brightness of the cluster. The resulting *uz*, *vz*, *bz*, *yz* photometry (all colors refer to half-light values) is listed in Table 1, where column (1) is the NGC number of the cluster, column (2) is the $uz-vz$ color, column (3) is the $bz-yz$ color, column (4) is the $vz-yz$

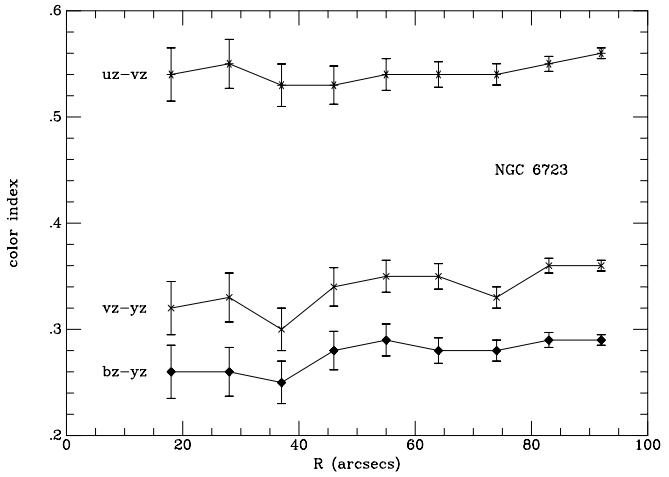

FIG. 2.—Aperture colors as a function of radius for globular cluster NGC 6723. While there is a mild redward color gradient with radius, colors level off by the half-light radius (85″). Formal errors range from 0.005 to 0.015 mag depending on apparent luminosity.

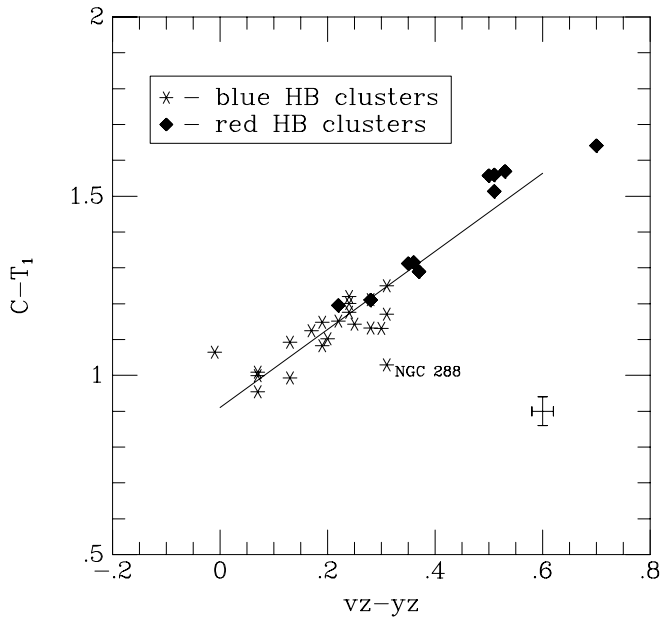

FIG. 3.—Washington metallicity index, $C - T_1$ vs. our metallicity index, $vz - yz$ for 32 globular clusters. The correlation is good, except for the anomalous cluster NGC 288. The solid line is a least-squares fit to the data (excluding NGC 288). There is no statistical difference between blue and red HB clusters (the second-parameter effect).

color, column (5) is the *mz* index, column (6) is the cluster age in gigayears (Salaris & Weiss 1998), column (7) is the mean cluster [Fe/H] (Harris 1996; Carretta & Gratton 1997), column (8) is the extinction $E(B-V)$ (Harris 1996), column (9) is the HB index (Lee, Demarque, & Zinn 1994), and column (10) is the $\Delta(bz-yz)$ index (see below).

A similar calibration to globular cluster metallicities was made with the Washington CMT_1 system by Geisler & Forte (1990). The Washington broadband filters covered 3910Å ($\Delta\lambda = 1100$ Å), 5085 Å ($\Delta\lambda = 1050$ Å) and 6330 Å ($\Delta\lambda = 800$ Å). The $C - T_1$ index is well calibrated to cluster [Fe/H] (Geisler & Forte 1990; Cellone & Forte 1996). From their study of 48 clusters, 30 overlap with our *uz*, *vz*, *bz*, *yz* photometry. Using our $E(B-V)$ values, their metallicity index $C - T_1$ and our $vz-yz$ index is plotted in Figure 3. The correlation between our systems is good even though the filter widths are dramatically different. This probably reflects the well defined stellar populations in globular clusters, in terms of a narrow turnoff and RGB sequences, as they convolve into color indices. Since the stars in a cluster have a narrow range in both age and metallicity, the resulting CMD is sharp and the contrast between clusters is clear to both narrow and broad band photometry. Notice, also, that there is no obvious difference between red and blue HB clusters (see below). One deviant cluster is NGC 288, a metal-rich system with a history of difficulty in defining its age from isochrone fits (also see below).

For calibration to a metallicity system, one would ideally like the total amount of heavy metals in a system, *Z*. Traditionally, the field of chemical evolution has used the ratio of iron and hydrogen normalized to the solar value, [Fe/H], as a direct tracer of *Z*. Globular cluster [Fe/H] measurements, based on isochrone fits, vary from author to author. While internal errors are quoted from 0.02 to 0.15 dex in the literature, a comparison between three metallicity systems (Zinn 1985; Rutledge, Hesser, & Stetson 1997; and Carreta & Gratton 1997) demonstrates a mean external error of 0.2 dex that we will adopt for our analysis. The [Fe/H] values used herein are listed in Table 1. We have also assumed that the spread of [Fe/H] within a cluster is less than our observational error, a fairly safe assumption given the narrowness of the giant branches in Milky Way clusters.

Metallicity in the *uz*, *vz*, *bz*, *yz* system is given by the $vz-yz$ index, which compares the light from a portion of the spectrum with several blends of metallicity indicators (Fe, CN) to a continuum region. The globular cluster relationship between [Fe/H] and our metallicity index, $vz-yz$, is shown in the top panel of Figure 4. The correlation is excellent with a formal linear fit given by

$$[\mathrm{Fe/H}]_{\mathrm{gc}} = 2.57 \pm 0.13(vz - yz) - 2.20 \pm 0.04$$

for the range of [Fe/H] of -2.5 to -0.5. There is a small gap around the [Fe/H] $= -1.0$ region, of critical importance for studying dwarf ellipticals. However, that region can be filled with [Fe/H] values determined spectroscopically for Fornax dE's (see § 2.3).

The correlation in Figure 4 is not due solely to line blanketing effects as would be the case for individual stars. There is a well-known shift in the effective temperature of the stars that make up the TO and RGB of the clusters as global metallicity of the stellar population vary. For this reason, the continuum index, $bz-yz$, also varies with metallicity, but with much greater scatter (shown in Fig. 5), indicating the importance of the line-blanketing component even in composite stellar systems. We note that the $vz-yz$ index varies both from temperature and line blanketing effects, which combine in the same direction (more flux in the *vz* relative to *yz* as the mean metallicity decreases) to tighten the correlation.

Of serious concern is the effect of age and horizontal-branch morphology on the metallicity calibration. The location of HB stars in the color-magnitude diagram (CMD) can vary from a position on the extremely blue edge of the instability strip (e.g., M13) to a red clump against the base of the giant branch (e.g., M3). Since M3 and M13 have similar metallicities, then some other parameter influences HB morphology (the so-called second-parameter problem).

TABLE 1

GALACTIC GLOBULAR CLUSTERS

Cluster (1)	$uz-vz$ (2)	$bz-yz$ (3)	$vz-yz$ (4)	mz (5)	Age (Gyr) (6)	[Fe/H] (7)	$E(B-V)$ (8)	HB Ratio (9)	$\Delta(bz-yz)$ (10)
104	+0.64	+0.28	+0.51	−0.05	9.2 ± 1.0	−0.70	0.04	−0.99	+0.067
288	+0.51	+0.31	+0.31	−0.31	8.8 ± 0.8	−1.07	0.03	+0.98	...
362	+0.58	+0.27	+0.37	−0.17	8.7 ± 0.8	−1.15	0.04	−0.87	+0.023
1851.....	+0.62	+0.26	+0.35	−0.17	7.9 ± 0.8	−1.22	0.02	−0.36	+0.052
1904.....	+0.60	+0.20	+0.22	−0.20	10.1 ± 1.1	−1.37	0.01	+0.89	+0.037
3201.....	+0.62	+0.27	+0.31	−0.23	9.9 ± 0.8	−1.23	0.21	+0.08	−0.010
4147.....	+0.58	+0.16	+0.13	−0.19	10.5 ± 0.5	−1.83	0.02	+0.55	+0.002
4372.....	+0.40	+0.14	+0.07	−0.21	11.5 ± 1.0	−2.09	0.50	+1.00	−0.020
4590.....	+0.53	+0.17	+0.07	−0.27	11.4 ± 1.0	−1.99	0.05	+0.17	−0.034
4833.....	+0.54	+0.18	+0.14	−0.22	...	−1.58	0.33	+0.93	...
5024.....	+0.50	+0.14	+0.13	−0.15	11.4 ± 0.5	−1.99	0.02	+0.81	−0.004
5053.....	+0.31	−0.04	−0.01	+0.07	...	−2.29	0.04	+0.52	...
5139.....	+0.53	+0.22	+0.24	−0.20	10.5 ± 0.5	−1.62	0.12	+0.75	−0.023
5272.....	+0.54	+0.21	+0.28	−0.14	10.1 ± 1.1	−1.34	0.01	+0.08	+0.032
5286.....	+0.56	+0.20	+0.19	−0.21	11.0 ± 0.5	−1.67	0.24	+0.80	−0.012
5466.....	+0.52	+0.07	−0.01	−0.15	...	−2.22	0.00	+0.58	...
5634.....	+0.49	+0.13	+0.19	−0.07	...	−1.82	0.05	+0.90	...
5897.....	+0.58	+0.22	+0.20	−0.24	10.1 ± 1.1	−1.59	0.09	+0.86	−0.019
5904.....	+0.52	+0.18	+0.24	−0.12	9.9 ± 0.7	−1.11	0.03	+0.31	+0.100
5986.....	+0.58	+0.22	+0.19	−0.23	...	−1.58	0.27	+0.97	...
6101.....	+0.57	+0.23	+0.17	−0.25	10.9 ± 1.1	−1.82	0.05	+0.84	−0.066
6171.....	+0.32	+0.20	+0.51	+0.11	10.4 ± 1.0	−1.04	0.33	−0.73	...
6205.....	+0.50	+0.20	+0.25	−0.17	10.3 ± 0.9	−1.39	0.02	+0.97	+0.034
6218.....	+0.44	+0.17	+0.28	−0.06	10.5 ± 1.0	−1.48	0.19	+0.97	+0.049
6229.....	+0.52	+0.19	+0.31	−0.07	9.5 ± 0.5	−1.43	0.00	+0.24	+0.038
6254.....	+0.32	+0.18	+0.30	−0.06	10.1 ± 1.1	−1.41	0.28	+0.98	+0.051
6352.....	+0.67	+0.30	+0.53	−0.07	9.4 ± 0.6	−0.64	0.21	−1.00	+0.057
6397.....	+0.54	+0.16	+0.07	−0.25	11.4 ± 1.1	−1.82	0.18	+0.98	+0.004
6584.....	+0.56	+0.21	+0.22	−0.20	10.1 ± 1.0	−1.49	0.10	−0.15	+0.008
6652.....	+0.66	+0.29	+0.50	−0.08	8.0 ± 1.1	−0.96	0.05	−1.00	+0.034
6656.....	+0.48	+0.27	+0.31	−0.23	...	−1.48	0.34	+0.91	...
6681.....	+0.52	+0.25	+0.25	−0.25	...	−1.51	0.07	+0.96	...
6715.....	+0.50	+0.25	+0.33	−0.17	...	−1.59	0.14	+0.87	...
6723.....	+0.56	+0.26	+0.36	−0.18	9.7 ± 0.5	−1.12	0.05	−0.08	+0.018
6752.....	+0.54	+0.21	+0.17	−0.25	9.6 ± 1.1	−1.42	0.04	+1.00	+0.019
6760.....	−0.12	+0.32	+0.70	+0.06	9.2 ± 0.5	−0.52	0.77	−1.00	+0.056
6809.....	+0.72	+0.21	+0.20	−0.22	12.0 ± 1.0	−1.81	0.07	+0.87	−0.044
6864.....	+0.62	+0.25	+0.35	−0.15	...	−1.32	0.16	−0.42	...
6981.....	+0.62	+0.25	+0.28	−0.22	...	−1.40	0.03	+0.14	...
7089.....	+0.63	+0.22	+0.24	−0.20	...	−1.62	0.02	+0.96	...
7099.....	+0.58	+0.15	+0.07	−0.23	11.5 ± 1.0	−1.91	0.03	+0.89	−0.001

NOTE.—Col. (1): Cluster NGC number. Col. (2): extinction corrected uz−vz color. Col. (3): extinction corrected $bz-yz$ color. Col. (4): extinction corrected $vz-yz$ color. Col. (5): extinction corrected mz index. Col. (6): cluster age in gigayears (Salaris & Weiss 1998). Col. (7): mean cluster [Fe/H] from Carretta & Gratton 1997 or Harris (1996). Col. (8): $E(B-V)$ from Harris (1996). Col. (9): horizontal-branch index from Lee et al. (1994). Col. (10): the age index, $\Delta(bz-yz)$ (see text).

To first order, the addition of another blue component would drive the $vz-yz$ metallicity estimate to lower [Fe/H] values. And, since [Fe/H] and HB morphology are correlated in the same direction (i.e., bluer population for lower metallicity), then it is possible that the metallicity calibration is distorted by HB morphology and the calibration would disappear in populations with a mixture of blue and red HB stars.

To determine the effect of HB morphology on the metallicity calibration, we have plotted blue and red HB clusters in the bottom panel of Figure 4. To make this division, we have assigned clusters with HB ratios, given by $(B-R)/(B+V+R)$ (Lee, Demarque, & Zinn 1994), of less than 0.1 the designation of red and those with HB ratios greater than 0.1 the designation of blue. The first parameter effect, that red HB clusters have higher metallicities, is obvious. In the overlap region, there is no trend to separate the sequences by $vz-yz$ color. Even M3 and M13, the extreme examples of HB morphology, are located within their photometric errors of each other on the calibration line. A similar lack of separation by HB morphology in $bz-yz$ as shown in Figure 5.

The lack of a second-parameter effect to the $vz-yz$ index is surprising since the uz, vz, bz, yz system is centered in the blue portion of the spectrum and should be sensitive to effects of bright, blue stars. There are two possible competing effects to the HB morphology that minimizes their influence on the metallicity index $vz-yz$. One is that blue HB stars are extremely hot and emit most of their energy in the UV. Their spectral energy distribution across the vz and yz spectral regions are much less than expected for their bolometric luminosities. Thus, clusters with a developing

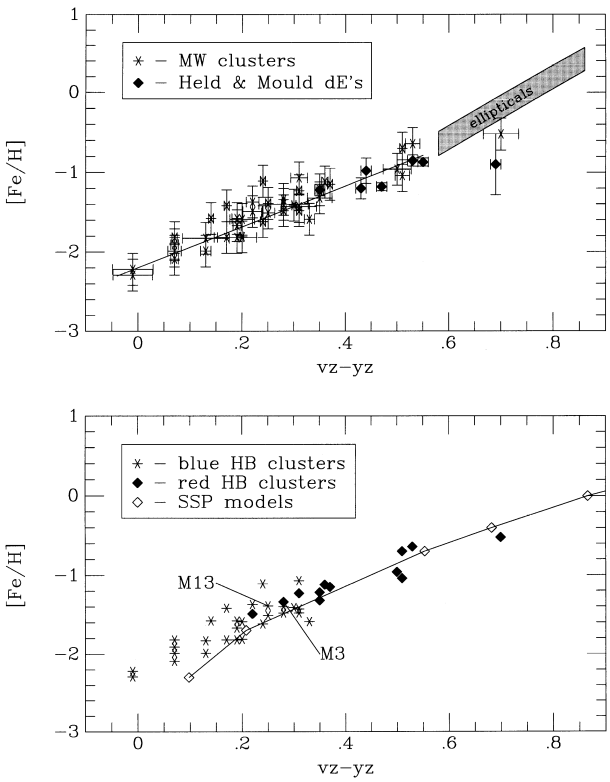

FIG. 4.—Metallicity color, $vz-yz$, vs. [Fe/H] for the 41 globular clusters listed in Table 1 (*asterisks*) and the Fornax dwarf ellipticals (*filled diamonds*) with spectroscopic measurements of [Fe/H] (Held & Mould 1994). The shaded region is the color-magnitude relation from Schombert et al. (1993) calibrated to the Kuntschner (2000) mass-metallicity relation. The bottom panel displays the globular cluster data divided into those with blue and red HB branches (separated by Lee index, Lee et al. 1994). M3 and M13, two extreme HB morphology clusters, are indicated. There is no evidence that the second-parameter effect distorts the metallicity calibration. The 13 Gyr SSP model of BC2001 is also shown.

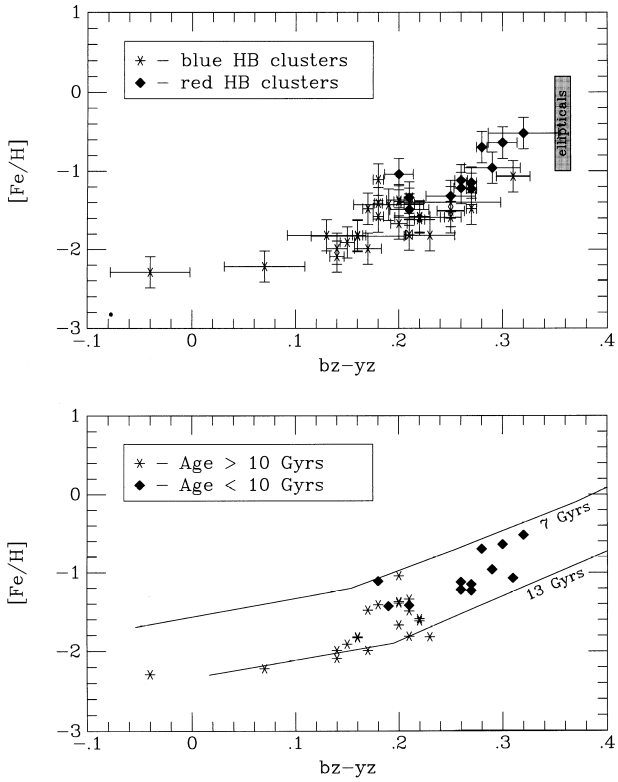

FIG. 5.—Continuum color, $bz-yz$, vs. metallicity [Fe/H] for the Milky Way globular clusters. The top panel displays the cluster data divided by HB morphology as per Fig. 4. The bottom panel displays the data for those clusters with isochrone ages (Salaris & Weiss 1998) along with two model tracks at 7 and 13 Gyr from BC2001. The shaded box in the top panel represents the run of $bz-yz$ color and metallicity for bright ellipticals.

blue HB component simply contribute less light to the $vz-yz$ as red HB clusters. This dropout of blue HB clusters is also seen in the Washington CMT_1 photometry system (Geisler & Forte 1990).

Secondly, and perhaps more important, is that the *uz*, *vz*, *bz*, *yz* filters are dominated by main sequence and RGB stars. The contribution from HB stars is less than 5% of the integrated light for an old stellar population (Guiderdoni & Rocca-Volmerange 1987). Based on comparison with SSP models, changes in the turnoff point and RGB populations, even small ones, have a larger effect on *uz*, *vz*, *bz*, *yz* colors than the HB morphology. The result is that metallicity calibration, to first order, appears free from distortions due to blue HB stars.

Changes in the age of a SSP are reflected in the location of both the TO and RGB populations in the CMD. However, the RGB shifts only slightly compared with the color of the TO population because of the relative contributions of the TO and RGB to near-blue portion of the spectrum (see Stetson, Vandenberg, & Bolte 1996). Calibration with age is more difficult with photometric systems because of the well-known age-metallicity degeneracy, since an age change produces an identical change in colors or spectral indices if the $\Delta \log \mathrm{Age}/\Delta \log Z = -3/2$ (Worthey 1994). With respect to the *uz*, *vz*, *bz*, *yz* system, age effects at constant metallicity reflect changes in the turnoff point of the composite CMD relative to the RGB contribution. In particular, for constant metallicity, the RGB changes only slightly with age (blueward) compared with relatively large changes in the color of the turnoff stars. Our method for resolving the age-metallicity degeneracy is to determine the expected $bz-yz$ color from the $vz-yz$ color (since age has little effect on the $vz-yz$ metallicity calibration) and correlate the residuals from expected and observed $bz-yz$ with age.

This age effect can be partially seen in the bottom panel of Figure 5, the plot of $bz-yz$ versus [Fe/H]. The scatter with metallicity is much higher compared with $vz-yz$. The bottom panel plots the expected $bz-yz$ color versus metallicity for a 7 and 13 Gyr population from Bruzual & Charlot models. Even though the isochrone ages have at least 0.5 Gyr of internal error, it is clear that much of the scatter in Figure 5 is due to an age difference (younger clusters being too blue for their [Fe/H] values). While this limits the use of the $bz-yz$ index for metallicity calibration, it does open up the possibility of using the residuals in $bz-yz$ to estimate age.

The first step in an age calibration is the correlation of $bz-yz$ with $vz-yz$. This correlation is good and connects with the previous correlation of ellipticals (Rakos et al. 1996). There is more scatter in $bz-yz$ with respect to the metallicity of the cluster, but this is expected since the *bz* and *yz* filters are in a featureless portion of the spectrum and correlate with metallicity only as it changes the mean effective temperature of the underlying stellar population. Our procedure, once the correlation between $vz-yz$ and $bz-yz$ is known, is to use the knowledge provided by the

metallicity index, $vz-yz$, which is relatively free from age and second-parameter effects, to fix the metallicity color of an object. Then we use the correlation between $vz-yz$ and $bz-yz$ to predict the expected $bz-yz$ index for the metallicity in question. Any residuals between the expected $bz-yz$ color and the actual observed $bz-yz$ color should measure changes due solely to the age of the underlying population (or recent star formation, which we ignore for the present).

The globular cluster residuals in $bz-yz$, designated $\Delta(bz-yz)$, are plotted in Figure 6 with respect to cluster age. For this study, we have used the new age determinations presented by Salaris & Weiss (1998). These new age determinations incorporate the latest changes in stellar physics, such as the equation of state and opacities, and also use the *Hipparcos*-based distances to the clusters. Their new calibration finds the age of the oldest globular clusters to be approximately 12 Gyr, in line with determinations of the age of the universe from cosmological constants. Comparison of age values from other work (Stetson et al. 1999; Carretta et al. 2000) requires the addition of 4.5 Gyr to Salaris & Weiss values.

For clarity, the age data for clusters from Table 1 have been divided into six bins of five clusters each. The error bars in Figure 6 display the range of $\Delta(bz-yz)$ and age. The correlation evident in Figure 6 is weak, mostly because of combined errors in the age determination and photometric corrections, but sufficient to estimate SSP ages at the 1 Gyr level and results in the following calibration:

$$T_0 = -33.97 \times \Delta(bz - yz) + 10.72 ,$$

where T_0 is the age of the cluster in gigayears. Note that the anomalous cluster NGC 288 is dropped from the age analysis because it displays discrepant age indicators. While Salaris & Weiss determine NGC 288's age to be 8.8 Gyr, other determinations (based on isochrone fits) are 2 to 3 Gyr older (e.g., Alcaino, Liller, & Alvarado 1997). In addition, NGC 288 is highly discrepant on the Washington calibration system (Geisler & Forte 1990), again suggesting a calibration problem for the cluster. The $\Delta(bz-yz)$ index indicates an age of 10 to 11 Gyr for NGC 288, more in line with other CMD ages; however, because of its poor isochrone fits, it was dropped from the above analysis.

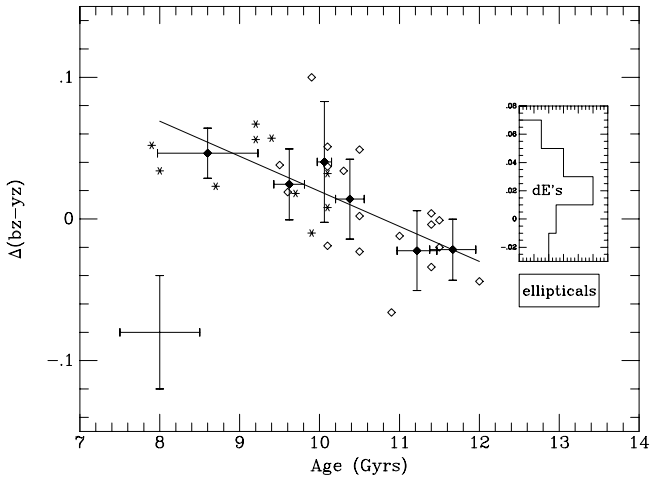

FIG. 6.—Residual color age indicator, $\Delta(bz-yz)$, vs. age in gigayears. The raw globular cluster data are divided by HB morphology from blue (*asterisks*) to red (*open diamonds*). Ages are from Salaris & Weiss (1998). A typical error for the globular colors and ages is shown in the bottom left corner. Average values (*filled diamonds*) are displayed along with a linear fit. The range for bright ellipticals ($M_B > -18$) is indicated. An inset histogram of $\Delta(bz-yz)$ values for the Fornax dwarfs is also shown. The $\Delta(bz-yz)$ values for bright ellipticals indicate a mean age of 13 Gyr, whereas the dwarfs have a mean age of 10 Gyr.

2.3. *SSP Models*

Globular clusters provide the simplest test to the SSP models since their stars are restricted in age and metal content. Galaxies, on the other hand, form their stars over some duration of time with the metallicity increasing for each new generation. For galaxies, the simplest model is one in which the total stellar population is composed of a series of SSPs assuming some metallicity distribution based on a chemical evolution scenario (Greggio 1997) and a star formation history (usually a single burst of a fixed duration for ellipticals). In order to investigate the effects of a composite stellar population with a range of metallicities (and ages) on the behavior of our color indices, we have adopted the SSP models of BC2001 with a Miller-Scalo IMF for the range of 0.1 to 100 $M_\odot$. The models follow a single-burst stellar population over a range of ages (1 to 17 Gyr) with a range of metallicities (1/200 to 2.5 times solar). A full description of the details of the modeling can be found in Liu, Graham, & Charlot (2000).

The BC2001 models are presented as a set of spectral energy distributions listing flux (ergs per square centimeter per second per angstrom) from 91 to 16000 Å. Our *uz*, *vz*, *by*, *yz* colors are determined by convolving the SEDs to our filter sensitivity curves (Rakos & Schombert 1995). At any particular epoch, the integrated SED of a galaxy will be composed of a series of populations of different metallicities and ages. What is observed will be the fluxed-weighted sum of the different populations. Because of this effect, the [Fe/H] value determined from the $(vz-yz)$ color will be in error if the distribution of real metallicities is not Gaussian. In order to determine the effect of a luminosity weighted metallicity, a particular model of chemical evolution is required. To this end, we have used the simple (vs. infall) model of Kodama & Arimoto (1997). This model assumes a closed box scenario (e.g., Gibson & Matteucci 1997) where the gas is well-mixed and uniform. The gas is enriched by ejection of metals from dying stars and succeeding populations are born from the enriched gas. This process continues until some event, such as galactic winds, halts the star formation process. While there may be complicating factors (such as initial enrichment or infall of gas-poor clouds), this model provides the most direct test of our assumptions and we will argue that changes in the basic assumptions make little difference to the resulting colors.

The bottom panel of Figure 7 displays the metallicity distribution required to fit the mass-metallicity sequence of ellipticals (Kodama & Arimoto 1997). The simple model results in a distribution of stars per metallicity given in Table 2. It has a peak at [Fe/H] = 0.5, but the numerical mean is 0.21, and most importantly the luminosity weighted [Fe/H] value is −0.10. To simulate a sequence of decreasing metallicity in galaxies, we have compressed the Kodama & Arimoto distribution by fractions, f_m, from the peak value of +0.5 dex (mean [Fe/H] = 0.21). Computationally, the lowest bin is fixed at [Fe/H] = −2.3 and the metallicity distribution is multiplied by f_m. This has the effect of lowering the mean metallicity while maintaining the shape of the distribution. We prefer this method, versus simply shifting

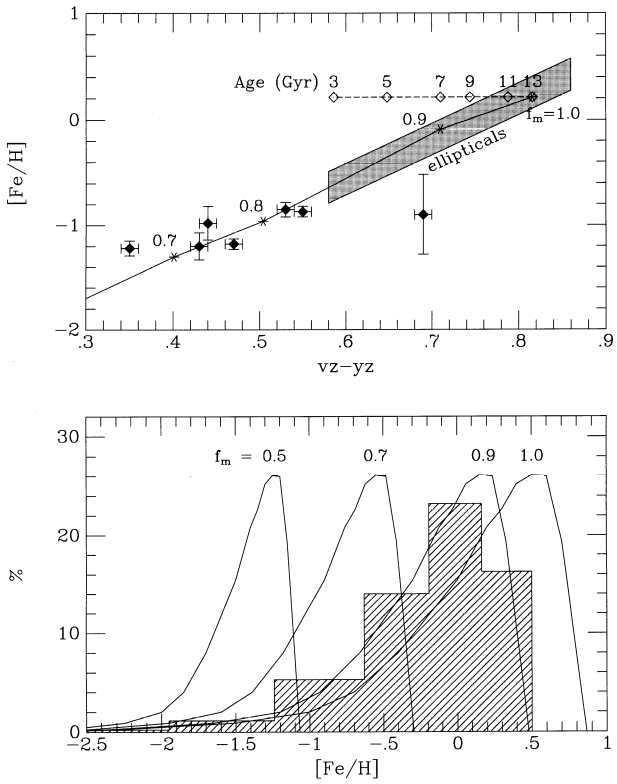

FIG. 7.—Multimetallicity populations in $vz-yz$, [Fe/H] space. The bottom panel displays the Kodama & Arimoto (1997) metallicity distribution for a standard elliptical model ($f_m = 1.0$). Lower metallicity models are produced by reducing the standard elliptical model by a constant (f_m). The quantization to the BC2001 models ([Fe/H] = −2.3, −1.7, −0.7, −0.4, 0.2, and 0.5) is shown as the shaded histogram for the $f_m = 0.9$ model. The top panel shows the resulting $vz-yz$ colors and luminosity weighted mean metallicity for the various f_m values. The shaded region is the color-metallicity relation from Schombert et al. (1993) using the Kuntschner (2000) calibration. The Held & Mould (1994) spectroscopic data on dwarf ellipticals (*filled diamonds*) are also shown. In addition, the dashed line shows the $f_m = 1.0$ model for various ages. The multimetallicity models are an excellent fit to the bright and dwarf elliptical data, in contrast to the clear discrepant nature to the bright ellipticals from the globular cluster relation in Fig. 4.

the metallicity distribution to lower values, since it maintains the sparseness of metal-poor stars per unit volume (the G-dwarf problem) as is observed in real galaxies (Worthey, Dorman, & Jones 1996). Three such compressed distributions are shown in Figure 7 and listed in Table 2. The resulting average metallicity of these distributions is given by the formula $\langle[Fe/H]\rangle = 5.51 f_m - 5.23$. Since the Bruzual & Charlot models are sorted in [Fe/H] bins of −2.3, −1.7, −0.7, −0.4, 0.0, and +0.4, the Kodama & Arimoto distribution is quantized by those values (shown as the shaded histogram for $f_m = 0.9$ in Fig. 7).

For each generated metallicity distribution, the appropriate population from the BC2001 models are assigned, weighted, and summed to produced the total flux for the integrated population. The resulting $vz-yz$ colors for a 13 Gyr population are shown in the top panel along with the color-magnitude relation for bright ellipticals (in this paper we refer to bright ellipticals as those galaxies with total luminosities greater than L^*) and data from Held & Mould (1994) for seven Fornax dE's where there is $vz-yz$ data to match the spectroscopically determined [Fe/H] values. The color-magnitude relation will be discussed in greater detail in § 2.5. In brief, the observed color-magnitude relation in $vz-yz$ is converted to the [Fe/H] scale using the relation of magnitude-[Fe/H] from Kuntschner (2000). Figure 7 confirms that the simple metallicity model outlined above precisely reproduces the $vz-yz$ versus metallicity relationship for globular clusters, dwarf galaxies, and bright ellipticals.

The result of the model comparisons is that the raw $vz-yz$ color of a galaxy with a composite stellar population will underestimate the real metallicity if the globular cluster calibration is applied without correction for the metallicity distribution of the underlying stellar population. For example, the $vz-yz$ color of the $f_m = 1.0$ model would have produced a luminosity-weighted [Fe/H] from the globular cluster calibration of −0.10 dex, whereas the real mean [Fe/H] value was +0.2 dex. In order to determine the mean metallicity of a galaxy, we must correct the luminosity-weighted color as guided by the model results. This multimetallicity correction is shown in Figure 8 for both 13 and 10 Gyr models. There is only a minor difference as a function of age, so we adopt a linear fit to the 13 Gyr correction,

TABLE 2

MULTIMETALLICITY MODELS

f_m	1.0 (percent)	0.9 (percent)	0.8 (percent)	0.7 (percent)
[Fe/] = −2.3.....	0.8	1.0	1.4	1.9
[Fe/] = −1.7.....	2.8	3.9	6.3	12.6
[Fe/] = −0.7.....	7.8	14.8	29.7	60.5
[Fe/] = −0.4.....	11.8	21.0	37.6	25.0
[Fe/] = 0.0	24.5	39.9	25.0	0.0
[Fe/] = +0.4.....	52.3	19.4	0.0	0.0
⟨[Fe/H]⟩	+0.21	+0.00	−0.34	−0.65
$[Fe/H]_{vz-yz}$.....	−0.10	−0.37	−0.65	−0.91

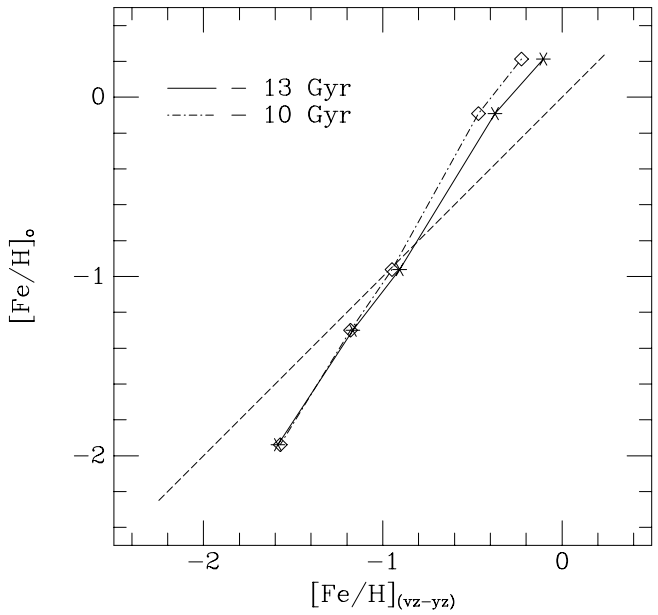

FIG. 8.—Observed [Fe/H] value vs. the true [Fe/H] from the multimetallicity models. The correction curve is shown for two ages, 10 and 13 Gyr. In general, the [Fe/H] value determined from $vz-yz$ based on the globular cluster calibration will underestimate the true [Fe/H] owing to contributions from stellar populations with a range of metallicities above [Fe/H] = −1 and overestimate below −1. The effect of age on the corrections is minor.

such that

$$[\mathrm{Fe/H}]_0 = 3.78 \pm 0.14(vz - yz) - 2.83 \pm 0.04 ,$$

where $[\mathrm{Fe/H}]_0$ is the mean metallicity of the entire population. We have also examined other metallicity distributions, such as the infall model of Kodama & Arimoto (1997), and they produce negligible differences in our results.

2.4. *Fornax Dwarf Ellipticals*

The observations of the Fornax dwarf ellipticals were made at CTIO using the 0.91 m Curtis Schmidt telescope plus STIS 2K CCD with 21 μm pixels. The plate scale of $2''.1$ pixel^{-1} covers $76' \times 76'$ of sky. The dE's were selected from the Ferguson catalog with high probability of membership based on morphological criteria (Ferguson 1989). While membership based on morphology may be questionable for most Hubble types, dwarf ellipticals have a particular appearance on photographic material (low surface brightness, exponential luminosity profile) that easily distinguishes them from background ellipticals. Membership is found to be good to 98% in both Virgo and Fornax using this method (Ferguson & Binggeli 1994). Two examples from our sample are shown in Figure 9, FCC 116 and FCC 207. They cover the range of surface brightness typical for our sample, although there exist many dwarf ellipticals with much lower surface brightnesses and the sample is not complete with respect to luminosity density.

Reduction and calibration followed the same procedures used for the globular clusters. Individual exposures for the dE's were long (typically 300 to 600 s) and co-added to remove cosmic-ray artifacts. Because of the plate scale of the Curtis Schmidt, none of the dE's were more than 5 to 10 pixels in radius which prevented a full surface photometry analysis of their colors. Values quoted are based on aperture magnitudes of 16 kpc metric size which is sufficient to contain the entire visible area of the galaxy. The reddenings of dwarfs were calculated according to Rakos et al. (1996) and assuming $E(B-V) = 0.03$ for the Fornax cluster (Hanes & Harris 1986). Results for the observed 27 dE's are listed in Table 3. The distance to Fornax assumed to be 18.6 Mpc (Madore et al. 1999).

All the dE's selected for this study are of the nucleated type (dE,N; see Sandage, Binggeli, & Tammann 1985). This was due primarily to the need to compare our photometry with [Fe/H] values determined spectroscopically in dE's. Because of their low surface brightness nature, only nucleated objects have been subjected to spectroscopy. While this may bias our results if the existence of a nucleus is an indication of recent star formation, broadband color studies indicate no difference between the color of the nuclei and the envelopes of dwarfs (Caldwell & Bothun 1987). The central peak appears to be of dynamical origin rather than a star formation event. In addition, dE's exhibit very little in the way of color gradients (Bothun & Mould 1988) that might distort our color indices with respect to mean metallicity.

A check of our globular cluster metallicity calibration directly to dwarf ellipticals is possible through the spectroscopy data from Held & Mould (1994). There are seven objects with both spectroscopy and *uz*, *vz*, *bz*, *yz* photometry (FCC 85, 150, 188, 207, 245, 266, and 296). All seven are plotted in Figure 4 using the median [Fe/H] values from Table 4 of Held & Mould. Notice that the Held & Mould dE's conveniently cover the intermediate-metallicity range between metal-poor halo globular clusters and metal-rich disk clusters. The dE $vz-yz$ colors are also in the region where the multimetallicity corrections from the equations in § 2.3 are small. All the Held & Mould dE's follow the same relationship as the globular clusters, within their errors, even without the multimetallicity corrections discussed in § 2.3. The reddest dE (FCC 85) has the largest [Fe/H] uncertainty, but still falls on the cluster sequence

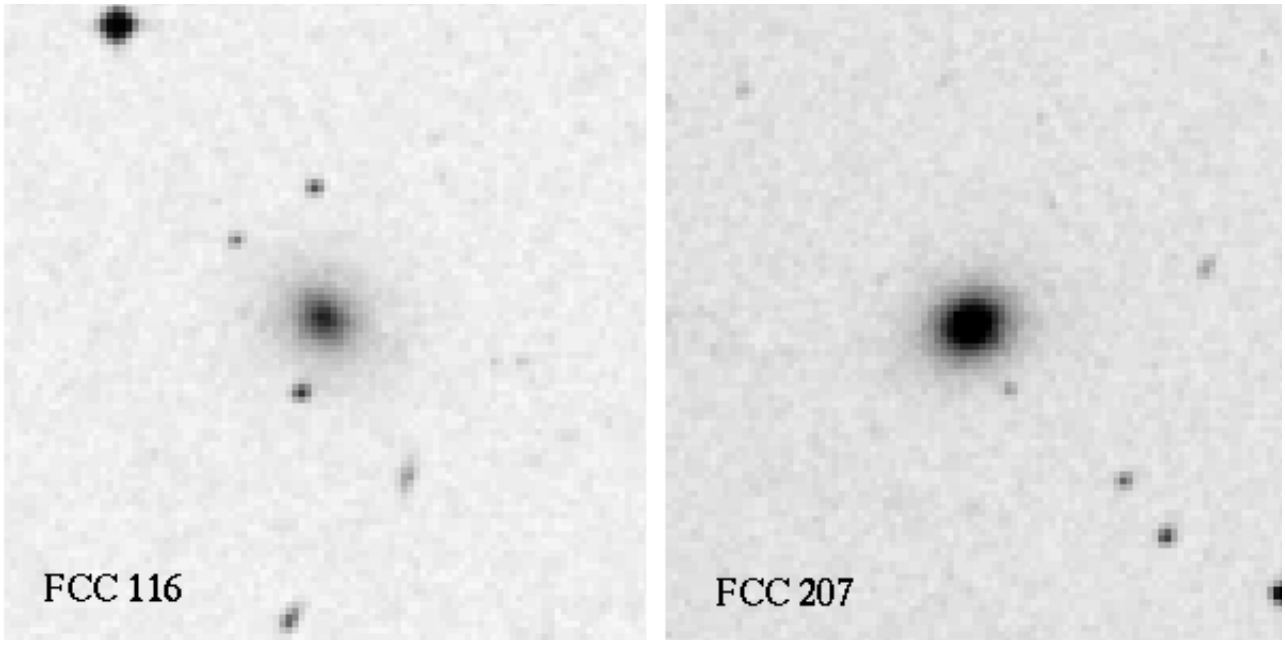

FIG. 9.—Two examples of the Fornax dwarf ellipticals in the sample. On the left is FCC 116, a low surface brightness dwarf, and on the right FCC 207, a high surface brightness dwarf. Each image is 3′ in width.

TABLE 3

FORNAX DWARFS

FCC (1)	$uz-vz$ (2)	$bz-yz$ (3)	$vz-yz$ (4)	mz (5)	[Fe/H] (6)	B_T (7)	$\Delta(bz-yz)$ (8)
85.....	0.31	0.39	0.70	1.01	−0.08	16.3	+0.027
116....	0.44	0.37	0.65	1.09	−0.09	16.9	+0.024
133....	0.36	0.38	0.49	0.85	−0.27	14.8	−0.058
136....	0.24	0.35	0.64	0.88	−0.06	16.1	+0.039
137....	0.17	0.43	0.58	0.75	−0.28	17.5	−0.068
150....	0.62	0.25	0.55	1.17	+0.05	15.7	+0.098
157....	0.42	0.23	0.37	0.79	−0.09	18.3	+0.037
160....	0.67	0.35	0.53	1.20	−0.17	17.7	−0.011
178....	0.72	0.28	0.46	1.18	−0.10	17.2	+0.027
181....	1.14	0.28	0.22	1.36	−0.34	17.2	−0.080
188....	0.74	0.34	0.47	1.21	−0.21	16.1	−0.027
189....	0.30	0.22	0.42	0.72	−0.02	18.8	+0.070
195....	0.77	0.27	0.39	1.16	−0.15	16.7	+0.006
202....	0.68	0.30	0.50	1.18	−0.10	15.3	+0.025
203....	0.67	0.29	0.46	1.13	−0.12	15.5	+0.017
207....	0.60	0.24	0.35	0.95	−0.13	15.9	+0.018
211....	0.59	0.28	0.35	0.94	−0.21	16.3	−0.022
222....	0.71	0.33	0.51	1.22	−0.15	15.6	+0.000
223....	0.94	0.26	0.36	1.30	−0.16	16.2	+0.003
230....	0.72	0.25	0.39	1.11	−0.11	17.2	+0.026
231....	0.68	0.30	0.52	1.20	−0.08	18.4	+0.036
245....	0.61	0.28	0.44	1.05	−0.12	16.0	+0.019
266....	0.66	0.34	0.53	1.19	−0.15	15.9	−0.001
274....	0.68	0.25	0.37	1.05	−0.13	16.5	+0.017
293....	0.90	0.29	0.46	1.36	−0.12	17.6	+0.017
296....	0.66	0.31	0.43	1.09	−0.19	16.3	−0.015
298....	0.60	0.28	0.39	0.99	−0.17	16.6	−0.004

NOTE.—Col. (1): FCC number. Col. (2): extinction corrected $uz-vz$ color. Col. (3): extinction corrected $bz-yz$ color. Col. (4): extinction corrected $vz-yz$ color. Col. (5): extinction corrected mz color. Col. (6): color determined [Fe/H], corrected to our multimetallicity models. Col. (7): apparent blue magnitude taken from Ferguson (1989). Col. (8): the age index, $\Delta(bz-yz)$.

within its error. From the fact that the global $vz-yz$ and spectroscopic [Fe/H] values are a good fit to the globular cluster relation in Figure 4, we conclude that total color measurements are in agreement with nuclear spectroscopy.

The distribution of $vz-yz$ and $bz-yz$ colors for the Fornax dE's can be seen in the histograms of Figure 10. The mean $vz-yz$ color is 0.46 ± 0.11, and the mean $bz-yz$ color is 0.30 ± 0.05. The $vz-yz$ colors transform into a corrected mean [Fe/H] value of -1.00 ± 0.28; however, the actual range of metallicities is from moderately metal-poor ([Fe/H] = −1.6) to values similar to metal-rich disk cluster ([Fe/H] = −0.4). This confirms what was found in optical, IR, and spectroscopy studies of dwarf ellipticals, that their metallicities are less than that of bright ellipticals and the disk of our own Galaxy, but greater than that of halo clusters (Bothun & Mould 1988).

The age of dwarf ellipticals can be estimated using the $\Delta(bz-yz)$ index discussed in § 2.1. Note that the age of composite SSPs, such as an elliptical galaxy, is the luminosity-weighted mean age of entire stellar population. If the star formation rate was proportional to the gas supply, then we would expect the SFR to be smooth function and the luminosity-weighted mean age to represent the time from the present to the time of peak star formation. For example, to estimate age for bright ellipticals we use the mean $vz-yz$ and $bz-yz$ values from Schombert et al. (1993). The ellipticals studied in Schombert et al. (1993) ranged from $vz-yz = 0.580$ to 0.885 (varying as the color-magnitude relation where fainter ellipticals were bluer) and this corresponds to expected $bz-yz$ values of 0.300 to 0.320. The measured $bz-yz$ values were 0.356 to 0.364, which then corresponds to $\Delta(bz-yz)$ values from −0.04 to −0.06 or 13 ± 0.5 Gyr (as shown in Fig. 6). This estimated age for bright cluster ellipticals would coincide with the values determined by spectral line studies (Trager et al. 2000) if corrected to the Salaris & Weiss cluster age system.

The range of $\Delta(bz-yz)$ values for Fornax dE's is shown as an inset in Figure 6. The mean $\Delta(bz-yz)$ for the dE's is 0.01 ± 0.04, which corresponds to a mean age of 10 Gyr with a range from 9 to 11 Gyr. While the accuracy on the $\Delta(bz-yz)$ index is low (since it is the difference of two colors and carries the photometric error, as well as the error to the globular cluster calibration), the mean is statistically different from bright ellipticals at the 99.9% level. The mean color of Fornax dE's indicates, at the very least, that dwarf

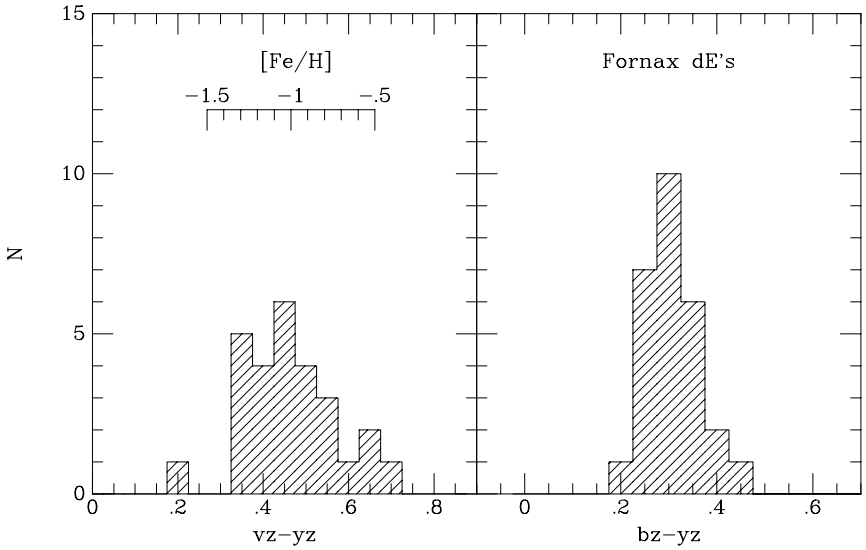

FIG. 10.—Histograms of $vz-yz$ and $bz-yz$ for the Fornax dwarf ellipticals. The calibration from $vz-yz$ to [Fe/H] from equations in § 2.4 is also shown. Dwarf ellipticals have a mean [Fe/H] of −1.0, ranging from −1.6 to −0.4. The mean $bz-yz$ color is 0.30 ± 0.05.

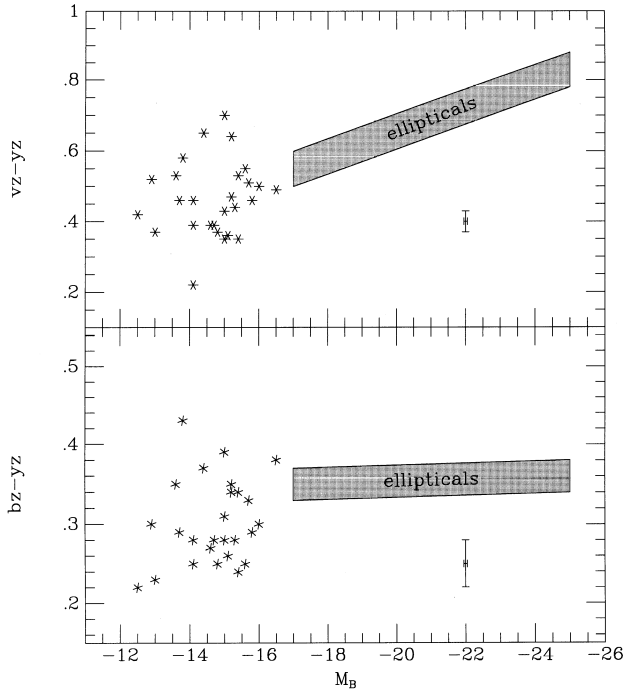

FIG. 11.—Color-magnitude relation for dwarf ellipticals. The shaded region is the CMR for bright ellipticals from Schombert et al. (1993). Typical error bars are indicated. The Fornax dwarf ellipticals do not appear to continue the tight CMR for more massive ellipticals in agreement with other studies.

ellipticals are younger than the oldest disk clusters in agreement with the age estimates based on the Balmer lines of Virgo dE's (Bothun & Mould 1988; Held & Mould 1994).

2.5. *Color-Magnitude Relation*

The relation between color and magnitude is well known (see Bower, Lucey, & Ellis 1992 and references therein) and is hypothesized to be a relationship between the stellar mass of a galaxy (luminosity) and the mean metallicity (color). Alternative explanations to the color-magnitude relation (CMR) that do not require metallicity effects have been proposed. One of the more viable scenarios is that the CMR is due to variations in age (Worthey 1994), but this hypothesis is not supported by Figure 7 (contingent on the various assumptions in the SSP models). The universality of CMR for the cluster environment has been demonstrated by Bower et al. (1992), and for the rest of this paper we will assume that the CMR is due to metallicity changes in the underlying stellar population.

Our best hypothesis for the origin of the CMR arises from the effects of galactic winds (Larson 1974). For a given unit of stellar mass, its mean metallicity is determined by the degree of past gas consumption. Since ellipticals have exhausted their gas supply, their metallicities should have identical values regardless of mass. Thus, the existence of a mass-metallicity relation (as reflected into the CMR) indicates that another process has altered the chemical evolution of ellipticals. Galactic winds have the right direction and magnitude in the sense that a galactic wind is delayed in more massive galaxies because of their deeper potential wells (Yoshii & Arimoto 1987; Tantalo et al. 1996). This results in stellar populations more enhanced in heavy elements and, therefore, redder in color. For low-mass galaxies, galactic winds result in a mean metallicity that is monotonic with mass. At higher masses, the yield flattens out at values around [Fe/H] = 0.3 (Mould 1984), which agrees well with the peak of the $vz-yz$, [Fe/H] relation in Figure 4.

In our previous work on bright ellipticals (Schombert et al. 1993), the CMR was determined for the *uz*, *vz*, *bz*, *yz* system. It is fairly strong for $vz-yz$ and weak for $bz-yz$, as expected for a metallicity change. Since that study, we have extended the CMR to higher luminosities from studies of distant clusters (Rakos et al. 2000). The CMRs for $vz-yz$ and $bz-yz$ are shown in Figure 11 along with the Fornax dE's. Immediately obvious from this diagram is that the dE's do not follow the same linear relationship as bright ellipticals. This is also seen in broadband colors (Caldwell & Bothun 1987; Prugniel et al. 1993), and it has been proposed that the lack of correlation is due to the possibility that dwarf ellipticals have an intermediate-age population. Interestingly, the spread in $bz-yz$ is just as large, compared with the bright elliptical sequence, as it was for $vz-yz$. Since $bz-yz$ is the most stable color with respect to evolutionary effects (Rakos & Schombert 1995), this hints at real differences in the underlying stellar population between dwarfs and more massive ellipticals, outside of an extrapolation of the metallicity sequence.

3. DISCUSSION

3.1. *α-Element Enhancement*

In Schombert et al. (1993), the zero point to the $vz-yz$ colors was linked to [Fe/H] through the Mg_2 index. This was done in part because the most direct measure of galaxy metallicity has traditionally been through the Mg_2 index, as it is one of the clearest spectral features in the optical portion of the spectrum owing to the dominance of G and K giant stars in galaxy stellar populations. The correlation between $vz-yz$ and Mg_2 was good, but a theoretical fit was required to obtain [Fe/H] from Mg_2. In our original study, we used the relationship from Worthey (1994) with the assumption of a [Mg/Fe] ratio of 0. However, the resulting [Fe/H] values for the cores of bright ellipticals were, on average, 0.3 dex too low compared with our estimates from their $J-K$ colors ($J-K$ measures the mean temperature of the RGB, also a metallicity-dependent feature in galaxies). The values for brightest ellipticals were also less than solar metallicities, which, since they are more massive than the Milky Way, was in conflict with our expectation of chemical evolution. We concluded in that study that the error was in the assumption that [Mg/Fe] was zero, and we predicted that there should be deficiency in Fe relative to Mg for our elliptical sample.

This deficiency between Fe and lighter elements, usually expressed as the [Mg/Fe] or [α/Fe] ratio, is known as the α-element enhancement, since the elements in question are all even atomic numbers synthesized by α-capture (see Worthey 1998). The problem with α-element abundance arises from the different methods in which light and heavy metal production occurs in a galaxy. Light α elements, such as Mg, and heavy elements, such as Fe, are both produced in Type II supernovae (SNe), the carbon detonation of a massive stellar core. Light and heavy elements are also produced by Type Ia SNe, the explosions due to accreting white dwarfs, but Type Ia SNe overproduce Fe relative to α elements in these events (from 2 to 10 times more Fe than

Type II SNe). Massive stars evolve quickly, and thus Type II SNe have very short lifetimes, on the order of a few to 100 million yr (Kobayashi et al. 1998). Type Ia SNe, on the other hand, require the companion to complete its slow evolution to the RGB and are estimated to have lifetimes from 0.6 Gyr to a few gigayears (Ishimaru & Arimoto 1997).

The different yield of Fe to lighter elements and the different timescales for Type Ia and Type II SNe allows for a range in [α/Fe] depending on their relative contributions to the galactic ISM. For example, the difference in timescales between Type Ia and II SNe would be evident in galaxies with initial episodes of star formation taking less than a gigayear, such that they will have chemical yields deficient in Fe compared with lighter elements (note that the ratio [α/Fe] is governed by the production, or lack thereof, of Fe, not α elements). Star formation that is prolonged over several gigayears will allow time for Type Ia SNe to inject additional Fe into the ISM for later generations of stars. In our own Galaxy, a shift in the [Mg/Fe] ratio is detected in metal-poor versus metal-rich field stars in the sense that older stars have enhanced [Mg/Fe], which slowly decreases to solar values as the stellar population becomes younger (Wheeler, Sneden, & Truran 1989), presumably reflecting the delayed enrichment of the Galactic ISM by Type Ia SNe.

The observational trend of [α/Fe] is difficult determine since it relies on high-S/N data of weak Fe lines (such as Fe 5270 and Fe 5335). Spectroscopy by Brodie & Huchra (1991) clearly shows that bright ellipticals have Mg_2 indices higher than expected from extrapolation of globular cluster values and Worthey, Faber, & Gonzalez (1992) demonstrate that the strength of the Fe 5270 and 5335 lines is weaker than expected for the Mg *b* line regardless of age or mean metallicity of the underlying stellar population. Fortunately, the direct evidence for a varying [Mg/Fe] ratio within ellipticals has improved dramatically in the last year. Both Trager et al. (2000) and Kuntschner et al. (2000) present Mg and Fe relations for more than 80 field and cluster ellipticals, demonstrating an increasing [Mg/Fe] ratio with galaxy mass (see their Figs. 6 and 12, respectively). The relationship appears independent of cluster environment and ranges from [Mg/Fe] = 0.3 for bright ellipticals ($M_B = -22$) to [Mg/Fe] = 0.1 for faint ellipticals ($M_B = -18$).

To investigate the run of [Mg/Fe] between globular clusters, Fornax dwarfs, and bright ellipticals, we have compared our $vz-yz$ values with Mg_2 values in the literature. The philosophy assumed here is that $vz-yz$ is coupled to the total metallicity of a stellar population (Z) through the behavior of the turnoff point and RGB colors, rather than weighted toward the α elements. This is not strictly true since isochrone shapes will change with varying [Mg/Fe] (Salaris & Weiss 1998), although the work of Tantalo, Chiosi, & Bressan (1998) concluded that change in [Mg/Fe] led to minor changes in the CMD of a SSP. Our analysis is further complicated by the practical consequence of calibrating $vz-yz$ to [Fe/H] rather than the total metallicity, Z, which actually determines color of the underlying stellar population. In order to investigate the magnitude of this problem, we have turned to the nonsolar abundance models of Weiss, Peletier, & Matteucci (1995). These models generate isochrones for [Mg/Fe] values of 0.0 and 0.45 over a range of metallicities, helium abundance, and mixing lengths. For our needs, it is sufficient to examine the change in $vz-yz$ color for varying [Mg/Fe] while holding all other variables, particularly [Fe/H], constant. When this experiment is performed, we find that $vz-yz$ varies by less than 0.01. This is a negligible amount, corresponding to only a change of 0.03 dex in [Fe/H] (see Fig. 7) or 0.1 Gyr in age. We note that recent work by Salasnich et al. (2000) finds that the turnoff of a 10 Gyr population will shift redward by $\log T_{\rm eff} = 0.011$ for a change in [Mg/Fe] of 0.4. This would correspond to a shift in $vz-yz$ of 0.04 or 0.1 dex in [Fe/H]. While this shift is larger than found in previous work, it remains small in comparison with other sources of error in our calibrations.

It is not too surprising to find that small changes in [Mg/Fe] have minor consequences for the integrated $vz-yz$ color. The multimetallicity model in Figure 7 assumes no color changes due to [Mg/Fe] changes, yet produces an excellent match to the $vz-yz$ versus [Fe/H] relation for bright ellipticals, despite a change from 0.1 to 0.3 in [Mg/Fe] (Trager et al. 2000; Kuntschner et al. 2000). In addition, the [Fe/H]-($vz-yz$) relation for ellipticals cannot be due to [α/Fe] effects, since the $vz-yz$ colors are too blue for their [Fe/H] values compared with SSP models or an extrapolation of the globular sequence. If α elements dominate the isochrones of the stellar population, then the colors of the brightest ellipticals (with the highest [α/Fe] values) would have colors redder than the extrapolation of the globular cluster sequence, which is clearly not the case in Figure 7.

The comparison between $vz-yz$ and Mg_2 for globular clusters, Fornax dwarfs, and bright ellipticals is found in Figure 12. The solid line represents the $vz-yz$, Mg_2 relation for ellipticals brighter than $M_B = -18$ adopted from Trager et al. (2000) and Kuntschner et al. (2000). The Mg_2 values for globular clusters and the Fornax dwarfs with

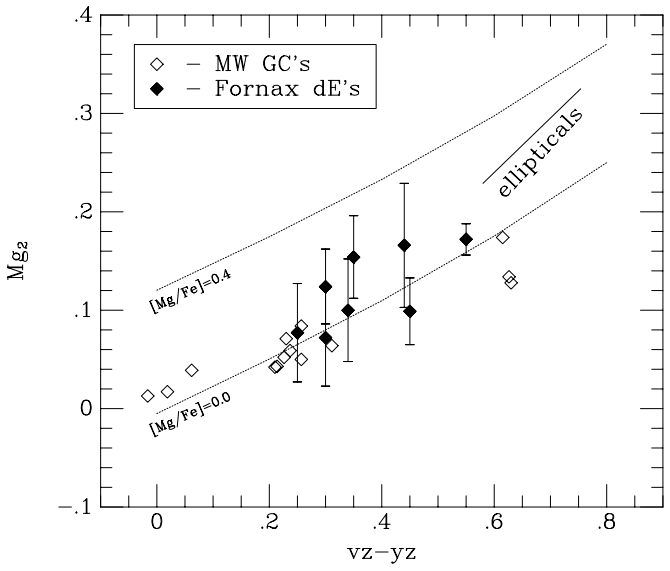

FIG. 12.—Mg_2 index vs. $vz-yz$ color. Globular clusters (*open diamonds*, Mg_2 indices are from Brodie & Huchra 1991) and Fornax dE's (*filled diamonds*, Held & Mould 1994) are shown The dashed line is the relationship between Mg_2 and $vz-yz$ for bright ellipticals from Schombert et al. (1993). Dotted lines are the curves of constant [Mg/Fe] from Weiss et al. (1995). While the dwarf elliptical data indicate slightly higher than solar [Mg/Fe], the bright ellipticals range from 0.1 to 0.3 dex. Globular clusters display a trend of decreasing [Mg/Fe] with metallicity, in agreement with their ages.

$vz-yz$ measurements are taken from Brodie & Huchra (1991). Also shown are curves of constant [Mg/Fe] taken from Weiss et al. (1995), with zero points set such that the top and bottom of the elliptical sequence corresponds to 0.3 and 0.1, respectively (Trager et al. 2000).

It is immediately clear that the dwarf ellipticals and globular clusters occupy the same region of Mg_2, $vz-yz$ space, although the scatter is high. The globulars follow a trend of decreasing [Mg/Fe] with increasing $vz-yz$ (i.e., [Fe/H]), as is expected from specific measurements of Galactic halo stars (Wheeler et al. 1989). For the globular clusters in Figure 12, the trend of increasing $vz-yz$ is also a trend of increasing age. Old clusters are enhanced in α elements because of the lack of enrichment by Type Ia SNe. Younger clusters, having formed several gigayears after the oldest globulars, have [α/Fe] values approaching solar.

The dwarf ellipticals lie in a region of the diagram that indicates they are an extension of the bright elliptical sequence to fainter magnitudes. Their position also indicates [α/Fe] values near or slightly above solar. This result is only preliminary and should be confirmed with direct measurement of Fe lines. Currently, the data in Figure 12 are consistent with the trend determined by Trager et al. (2000) of decreasing [α/Fe] with decreasing galaxy mass. We also note that, if confirmed, Figure 12 allows a crude measure of [α/Fe] in galaxies, which may be difficult to measure directly because of the intrinsic faintness or low surface brightness of weak Fe lines. For example, Mg_2 and $vz-yz$ would be easier to obtain in distant galaxies or LSB objects using only low-resolution spectroscopy.

The origin of the trends of [α/Fe] in Figure 12 is obscure. Clearly, the different yields of α elements and Fe from Type Ia and II SNe are the primary source for the variations with galaxy mass, unless some process can selectively remove light or heavy elements from the ISM. There are several different scenarios to produce the trend of [α/Fe] with galaxy mass (see Trager et al. 2000 for a fuller discussion). We will consider three possible scenarios in conjunction with the impact on the star formation history in dwarf ellipticals: (1) varying lengths in star formation duration, (2) different galactic wind strengths, and (3) variations in the initial IMF. The data presented in this section are insufficient to choose between these scenarios.

The most obvious explanation for the low [α/Fe] in dwarfs is that low-mass galaxies have longer periods of initial star formation, compared with high-mass ellipticals. A longer initial burst of star formation leads to a later epoch before the onset of galactic winds and, therefore, more time for Type Ia SN detonation and the increase in Fe abundance (see Worthey et al. 1992). However, the total elemental production is increased with longer durations of star formation, in contradiction with the color-magnitude relation, unless the strength of the initial burst also decreases, i.e., fewer generations per unit of time (see scenarios 1 and 2 of Trager et al. 2000). This make this hypothesis problematic with regard to the mass-metallicity relation (see § 3.2).

While star formation and SN production is the known method to produce heavy metals, a mechanism to halt star formation is required to produce the mass-metallicity relation in galaxies. Otherwise, closed-box models required that all galaxies have identical (and much great than solar) mean metallicities. The most plausible method to produce the mass-metallicity relation is to invoke galactic winds to halt star formation by removal of the ISM (see § 3.5). Certainly, the production of SNe during initial star formation provides the energy source for the heating of the ISM into a wind state. Higher mass galaxies would maintain deeper gravitational wells, which in turn requires more energy for a wind. More energy results in greater metal injection and higher mean metallicities for each generation of stars. With respect to [α/Fe] enhancement, the timing to the onset of a galactic wind and/or its strength can influence the ratio of retained α elements. For example, if the onset of a galactic wind were delayed, then the mean [α/Fe] value would decrease as more Type Ia SNe contribute to the ISM. Another possibility is if the wind varies in strength with galaxy mass. Then, low-mass galaxies would have weak winds that slow the depletion process allowing late enrichment by Type Ia SNe and thus lowering the mean [α/Fe].

Lastly, since α elements arise primary from massive stars, a varying IMF can result in different [α/Fe] values. In this scenario, high-mass galaxies are richer in massive stars during their early stages of star formation. This leads to a higher contribution from Type II SNe and an increase in [α/Fe] with galaxy mass (assuming that the time before galactic winds is longer than the timescale of Type Ia SNe). This idea is not without merit since higher mass galaxies have a higher number density of clouds and more violent cloud collisions. This type of star formation has been detected in galaxy mergers along with indications of a higher number of high-mass stars (Elmegreen et al. 2000). Additionally, an early enhancement of the IMF will not be detected in present-day galaxy colors since, if the changes involve only the highest-mass stars, then those stars have long since evolved out of the current visible stellar population.

3.2. *Mass-Metallicity Relation*

The key to understanding the chemical evolution of ellipticals is the relationship between galaxy mass and the mean metallicity of its stellar population. The CMR is just one manifestation of this effect and other correlations, such as with central velocity dispersion and metallicity lines or the Z hyperplane (Trager et al. 2000), are also present in ellipticals. To examine the mass-metallicity relation for dwarf galaxies, we have plotted [Fe/H] versus absolute blue magnitude (M_B) for Local Group dwarfs, Fornax dwarfs, and bright ellipticals in Figure 13. We have made two assumptions in the following interpretation of this diagram: (1) that [Fe/H] traces the total metallicity of a galaxy (Z) and (2) that the absolute blue magnitude traces the mass. The first assumption is supported by numerous line indices and gradient studies. The second assumption means that the M/L_B's are relatively constant between dwarfs and bright ellipticals. Bright ellipticals range in M/L_B from 4 to 10 (Kronawitter et al. 2000), but dwarf ellipticals are less well known. Peterson & Caldwell (1993) find at range of M/L_B from 1 to 7 for dE's in Fornax and Virgo. Population models estimate M/L_B in the range of 4 to 6 (Worthey 1994). We conclude that, within 20%, the blue magnitude traces the mass from dwarf to bright elliptical.

The shaded zone in Figure 13 represents the region of magnitude and metallicity outlined by the Brodie & Huchra sample (their Fig. 3, adjusted to an $H_0 = 75$). While displaying the known trend of decreasing [Fe/H] with mass, the region is notable for the increase in its metallicity range with lower elliptical luminosities. The dashed line represents the Schombert et al. (1993) CMR calibrated to [Fe/H] fol-

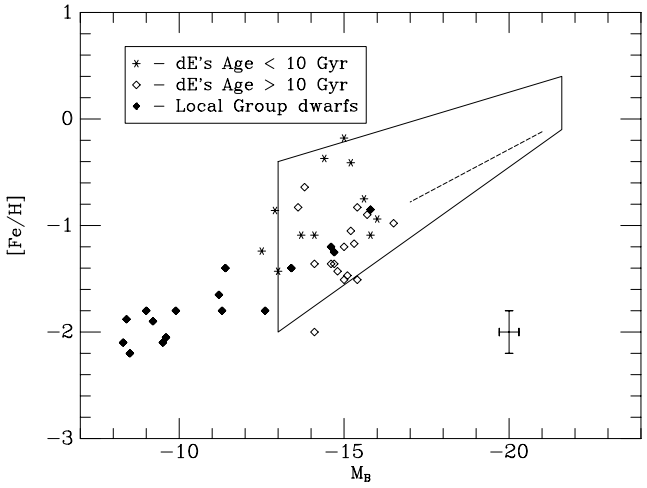

FIG. 13.—The mass-metallicity diagram for normal and dwarf ellipticals. The outlined region is the mass-metallicity relation from Brodie & Huchra (1991; their Fig. 4). The dashed line is the color-magnitude relation from Schombert et al. (1993). Fornax dwarf ellipticals with ages greater than 10 Gyr (*open diamonds*) are compared with Fornax dE's with ages less than 10 Gyr (*asterisks*). Local Group dwarfs (*filled diamonds*) from da Costa (1998) are also displayed. As the mass-metallicity relation broadens for low-luminosity ellipticals, there is a tendency for younger ellipticals to lie at the top of the sequence and the older galaxies to form the lower sequence.

lowing the prescription in § 2.3. Since our bright elliptical and distant cluster data sets do not sample below $M_B = -18$, we cannot test the validity of the increase in the range of [Fe/H] for low-luminosity ellipticals, except to note that other studies have confirmed this increase beyond what is expected for observation uncertainty. The data for Local Group dwarfs (da Costa 1998) are also shown in Figure 13.

By themselves, the Fornax dwarf data do not follow any mass-metallicity relation, as we would have expected from the scatter in the $vz-yz$ CMR from § 2.3. It is interesting to note that there is a group of Fornax dE's that follow the relationship defined by Local Group dwarfs and the CMR for bright ellipticals and a group that lies above the CMR with a distinct gap between them. This suggests that the spread in mass-metallicity may be due to a galaxy second-parameter effect, such as a dependence on the central velocity dispersion (Terlevich et al. 1981) or a range of star formation efficiency, where galaxies along the top of the sequence were highly efficient at converting gas into stars versus those galaxies along the bottom edge of the sequence. Another possible factor in the spread of metallicity would be some event, such as a merger or tidal collision, which removed gas and/or halted star formation.

Lacking dynamical information on our dwarf sample, we instead test the age of the Fornax dwarfs using the $\Delta(bz-yz)$ index. The sample is divided into those dwarfs with mean ages greater than 10 Gyr and those less than 10 Gyr, shown as different symbols in Figure 13. While there is no trend of [Fe/H] and age, it is clear that the younger dwarfs tend lie above the older dwarfs in the mass-metallicity diagram. Notice that the trend is opposite to what is expected from observational error in that the younger galaxies per luminosity bin have high [Fe/H] values (i.e., redder colors). Note also that younger galaxies are not necessarily bluer than the mean, but merely bluer than the other galaxies in their mass bin. This confirms what was noted by Bothun & Mould (1988) and Held & Mould (1994) that there is a range of Balmer line strengths in dE's at a fixed metallicity compared with globular clusters.

This trend between galaxy mean metallicity and age is understandable in terms of a simple model of chemical evolution. If cluster galaxies all form at the same epoch, then younger mean age implies a longer timescale for star formation and more time to recycle the ISM before the onset of galactic winds. Thus, per mass bin, one would expect the younger galaxies to have higher metallicities as younger age represents more time for the yield from SNe to increase the [Fe/H] for each stellar generation. We conclude that the mass-metallicity relation is distorted for dwarf ellipticals, not because of range of ages as it directly influences the CMR, but rather by the younger age galaxies having higher metallicities due to a longer history of chemical evolution.

3.3. *Mean Age of Dwarf Ellipticals*

In a recent study of 50 local field and cluster ellipticals, Trager et al. (2000) conclude that there is range of ages in field ellipticals (from 1.5 to 18 Gyr), but that cluster ellipticals tended to be old with a mean age between 10 and 13 Gyr. Kuntschner (2000) confirms the coeval nature of the cluster ellipticals in Fornax with a mean age of 13 Gyr using the Hβ versus Fe diagrams pioneered by Worthey (1994). Bressan, Chiosi, & Tantalo (1996), using a similar analysis, find that there must be age variations, in addition to metallicity changes, to explain the distribution of elliptical's 1550 Å colors, Hβ and Fe indices, but that all ellipticals are older than 6 Gyr. Certainly, in this study, the CMR of cluster ellipticals is well modeled by a luminosity-weighted metal distribution (see § 2.3) and the scatter in the CMR restricts the age spread to less than 2 Gyr for cluster ellipticals. In addition, studies that follow the color evolution of cluster ellipticals are well matched to models of passive evolution of their stellar populations to a redshift of formation of $z_g = 5$ (Rakos & Schombert 1995).

As mentioned in the introduction, the line indices methods have the greatest resolution of the age-metallicity degeneracy, but also carry the light element enhancement assumptions. The [α/Fe] values used by Trager et al. (2000) all were empirically determined from their own indices and those values are confirmed in § 2.3. However, an alternative to the line indices method of dating ellipticals is to examine the mean colors which measure the average position of the turnoff point (the change in the position of the RGB is relatively small for small changes in age). To this end, we have used the $\Delta(bz-yz)$ index as a direct measure of the mean age of bright and dwarf ellipticals through the color of the turnoff stars. To repeat the discussion in § 2.1, the $vz-yz$ index is less sensitive to age than to metallicity when compared with $bz-yz$. We can in effect predict the $bz-yz$ color based on the $vz-yz$ index. In terms of the underlying stellar population, this is equivalent of examining deviations of the turnoff point for a fixed metallicity. Negative $bz-yz$ residuals signal an older population; positive residuals signal a younger one. We have calibrated the $\Delta(bz-yz)$ index using globular clusters and SSP models; however, we caution the reader that ellipticals will have the broad turnoff points that one would expect from a burst of star formation extended in time (globular clusters form all their stars in very short timescales producing sharp CMDs). We note, for example, the color-magnitude diagram of the

Fornax dwarf spheroidal (Buonanno et al. 1999) has a wide RGB and main sequence, indicating an onset of star formation 12 Gyr ago with continuous bursts up to 0.5 Gyr ago.

In § 2.2, it was demonstrated that the $\Delta(bz-yz)$ index implies that dwarf ellipticals are about 3 Gyr younger than bright ellipticals in mean age. There is no evidence from their narrowband colors that cluster ellipticals have a range in age and the CMR suggests they are coeval with a mean age of 13 Gyr. The Fornax dwarfs, on the other hand, range in age from about 9 to 11 Gyr. There is a great deal of scatter in these values due to observational errors and the inherent uncertainties contained in our method, but the mean age for dwarfs is clearly much less than bright ellipticals. If the Fornax dwarfs' younger mean age is universally applicable to all dE's, then this would explain the spectroscopic observations of Virgo dwarfs by Bothun & Mould (1988). In that study, it was found that the Ca II K ratio was similar to metal-rich clusters such as 47 Tuc. However, the Balmer line strength was slightly stronger, indicating a younger age, younger than globular cluster ages. If we take the age of 47 Tuc to be 9.2 Gyr (Salaris & Weiss 1998), then a mean age for Fornax dE's of 9 to 10 Gyr would be in agreement with the spectroscopic data of Virgo dE's. In addition, both Thuan (1985) and Caldwell & Bothun (1987) found that the $B-H$ colors for dE's in Virgo are too blue relative to their $J-K$ index, again a signature of younger mean age.

One possible complication in our dating method is that it is possible that our colors may be reflecting a recent burst of star formation on top of an old stellar population. To test for recent star formation, we added 1% of a 1 Gyr population to a low-metallicity 13 Gyr population (so-called frosting models, Trager et al. 2000). The resulting colors would produce a 1 Gyr shift in the mean age as calculated by the $\Delta(bz-yz)$ index. Thus, the addition of 3% to 4% of a 1 Gyr population would be required to produce the mean ages observed in Figure 6. This would seem excessive given the lack of H I detection in dE's. The dwarf ellipticals in the M81 group, similar in mass to the Fornax dwarfs, display no evidence of a young population (less than 2 Gyr) from *HST* CMD diagrams (Caldwell et al. 1998). In addition, vacuum UV imaging places severe constraints in the number of OB stars in dwarf ellipticals (less than 1% contribution by a hot component, O'Neil et al. 1996) and, thus, we rule out recent star formation for dE's as a source of the bluer $bz-yz$ colors.

3.4. *Star Formation Duration*

It is difficult to determine from the present data, or from model fits, whether the younger mean age for in any galaxy is due to a later epoch of initial star formation (compared with bright ellipticals) or due to the effects of an extended duration of star formation. We can attempt to infer the duration of star formation based on the trend of [Mg/Fe] in § 3.1, but only if we assume that the change in α elements is due solely to the delay between Type Ia and Type II SNe. This section will focus on duration effects and other processes, such as galactic winds, will be considered in the next section.

To first order, a lower [Mg/Fe] value implies longer star formation timescales in order for Type Ia SN enrichment to occur. The change in [Mg/Fe], suggested in Figure 12, implies that bright ellipticals ($M_B > -18$) have a duration of initial star formation that is inversely proportional to their mass. The duration of star formation for low-mass ellipticals was long enough (a few gigayears) for Type Ia SNe to contribute to the mean metallicity with corresponding lower [Mg/Fe] values. Conversely, the duration of star formation for high-mass ellipticals must have been shorter resulting in higher [Mg/Fe] values. Under this interpretation, the Fornax dwarf ellipticals must have even longer duration times, compared with bright ellipticals, since there [Mg/Fe] values are close to solar.

In addition to the [Mg/Fe] information, we also have the age estimates from Figure 6 which indicates a mean age for dwarfs ellipticals of 10 Gyr, about 3 Gyr younger than bright ellipticals. This is consistent with the hypothesis of a longer duration of star formation compared with bright ellipticals as the younger mean age would then be reflecting a later epoch for the cession of star formation. Given the division by age in the mass-metallicity relation (Fig. 13), the star formation history of dwarf ellipticals may break into two sequences, an upper track with a longer duration (younger mean age) and a lower track with a shorter duration and colors that indicate an older population. This would predict that upper sequence dwarfs have enhanced [Mg/Fe] compared with upper sequence, but there are no data at this time to test this hypothesis.

The main difficulty in the interpretation of the [Mg/Fe] and mean age data, in terms of the duration of the initial burst of star formation, is the fact that longer timescales of star formation should imply higher metallicities. This was pointed out in Trager et al. (2000) that the trend of increasing [α/Fe] is at odds with the mass-metallicity relation for ellipticals. A shorter duration of star formation for high-mass ellipticals should result in less chemical evolution and, therefore, lower metallicities. Clearly, another mechanism is involved in the evolution of galaxy stellar populations, such as galactic winds.

3.5. *Galactic Winds*

Massive star formation ultimately leads to the injection of energy into the ISM through SNe and stellar winds. If the energy input exceeds the gravitational binding energy of the galaxy, then a galactic wind develops removing the remaining ISM (Larson 1974). Evidence for galactic winds is mostly indirect. They are needed to remove gas from ellipticals in a quick in timely fashion so that most present-day ellipticals are free of neutral gas (although they have large quantities of hot, X-ray emitting gas, presumingly the remnant of baryonic blowout). Since cluster elliptical colors indicate coeval star formation epochs with a sharp cutoff well over 10 Gyr ago (Rakos & Schombert 1995), galactic winds are the preferred method to cease star formation in a uniform fashion to cluster ellipticals as a class of objects. Galactic winds are also convenient for explaining the high heavy metal abundances of the intracluster medium (Arnaud et al. 1992). Ellipticals, again, are a likely source of this material since they are a major mass component of rich clusters of galaxies.

The mass-metallicity relation also requires some mechanism like galactic winds to explain the dependence of mean metallicity on the total mass of a galaxy. Regardless of mass, the mean metallicity of a region is governed by gas consumption. If star formation proceeds in ellipticals such that all the gas is converted into stars, then they should have high, and nearly constant, mean metallicities (i.e., closed box model). Clearly, cluster ellipticals are not of

uniform metallicity, as demonstrated by the CMR and spectral line studies. The onset of a galactic wind, as a function of mass, produces the proper correlation with the reasoning that high-mass galaxies have a higher gravitational potential which retains the gas for a longer amount of time allowing for higher enrichment. In this scenario, known as the classic wind model, the key parameter that determines the mean metallicity of a galaxy is the timescale before the onset of a galactic wind where longer timescales result in higher metallicities.

On the other hand, an early galactic wind, after short duration of star formation, may result in high metallicities if star formation is more efficient with higher galactic mass. This is opposite to classic wind scenario, called the inverse wind model (Matteucci 1992). In the inverse wind model, galaxy formation follows a different course than the assumed homogeneous collapse of a giant protogalactic gas cloud. Some process, for example mergers, produces higher densities and higher cloud collision rates than those resulting from pure dynamical timescales. This results in more massive galaxies developing an early galactic wind, but with a higher rate of star formation and corresponding higher rates of chemical evolution.

The key parameter in distinguishing between the classic and inverse wind model is the time between initial star formation and the onset of galactic winds, t_{gw}. For ellipticals, this is assumed to be equivalent to the duration of star formation since the galactic winds remove the ISM and halt subsequent star formation. Classic wind models assume that t_{gw} decreases with decreasing galactic mass. For example, Kodama & Arimoto (1997) reproduce the $V-K$ CMR using $t_{gw} = 0.5$ Gyr for the bright end, dropping to 0.1 Gyr for the faint end. The inverse wind model (Matteucci 1992) reverses the trend with a SF duration of 0.5 Gyr at the faint end dropping to 0.1 Gyr for galaxies with $M = 10^{12}\ M_{\odot}$. We note that the classic wind model is at odds with the observation that [α/Fe] decreases with galactic mass such that cession of star formation in 0.1 Gyr for faint ellipticals will not produce the [α/Fe] values near 0.1 seen by Trager et al. (2000) and Kuntschner (2000).

Some indication of the relative importance of star formation duration and onset of galactic winds is provide by the range of age for dwarf ellipticals in Figure 13, the mass-metallicity diagram. The dwarfs have a range of metallicities (from [Fe/H] $= -1.6$ to -0.4). A pure galactic wind model would predict early winds produce low-metallicity dwarfs and the onset of an early wind would also produce an older stellar population. Indeed, that is what is observed in Figure 13, the oldest dwarfs have the lowest metallicities, while the youngest dwarfs have the highest metallicities. A pure wind interpretation would also imply a similar rate of star formation (per unit mass) with a later epoch of winds providing the cutoff for mean age (younger for late winds) and a longer time for chemical evolution (higher [Fe/H]).

The problem with this simple wind model is that one would expect a correlation between dwarf mass and metallicity. An early wind implies a low gravitational potential and, thus, a lower mass dwarf compared with those which produced late winds. Therefore, we would expect to find a tight mass-metallicity correlation for dwarf ellipticals, which is not the case in Figure 13. Since neither star formation duration nor galactic winds are able to satisfactory explain the characteristics of dwarf ellipticals, we are led to speculate that external factor, such as the cluster environment, may have a controlling factor in the early star formation history of cluster dwarfs.

3.6. *Cluster Environment*

If bottom-up scenarios for galaxy formation are correct, then dwarf galaxies should exist as fossil remnants of the epoch of galaxy formation. Their metallicities would then provide the most direct look into the chemical history of a cluster, on the assumption that their current positions map into their dynamical past. Figure 14 displays the $vz-yz$ colors of the dwarfs as a function of radius from the core of the cluster (assumed to be the position of NGC 1399). There is a clear gradient in metallicity color from the core to the halo which corresponds to about 0.7 dex. Core metallicities are lower than halo metallicities (opposite to our own Galaxy) with a mean of [Fe/H] $= -1.3$, which then rises to a mean of [Fe/H] $= -0.6$ in the outskirts of the cluster.

This decrease in metallicity with decreasing radius is opposite to the expectations due to metallicity observations of the hot x-ray gas in clusters. ASCA measurements of the Fe K line for several rich clusters of galaxies indicates a drop from $\frac{1}{2}$ solar at the core to $\frac{1}{3}$ solar in the outskirts (Dupke & White 2000). In addition, the abundance ratios in the core intracluster gas suggests a strong Type Ia SN component (Dupke & White 2000). Since metals in the intracluster gas have two possible origins, galactic winds or ram-pressure stripping (Gunn & Gott 1972), the abundance ratio would rule out an origin for the gas strictly from matter ejected by early winds, which is primarily Type II SN enriched material. Later winds or stripping of Type Ia SN gas from bright ellipticals is required to balance the abundance ratios. We note, however, that this [α/Fe] ratio matches the expected ratios in dwarf ellipticals and, thus, they may contribute a large fraction of the intracluster gas.

If dwarfs are major contributors to the intracluster metals then there may be a feedback process involved such that the cluster environment is responsible for the dwarf metallicity

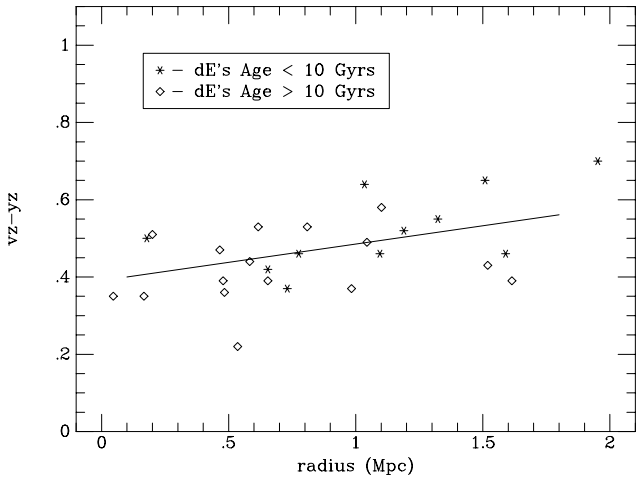

FIG. 14.—Fornax dwarfs $vz-yz$ color as a function of cluster radius. The Fornax dwarf ellipticals display a noticeable increase in metallicity with increasing cluster radius. This is opposite to the metallicity trend for the intracluster gas, which decreases with radius, and may indicate that dwarfs are a major source of metals to the intracluster gas. We also find that there is a weak correlation with galaxy mean age as a function of radius, such that older dwarfs inhabit the cluster core and younger dwarfs are found in the halo. This observation is consistent with the idea that the intracluster medium halts star formation and enrichment in dwarf galaxies through a ram-pressure stripping mechanism.

values. For example, the low [Fe/H] values of core dwarf ellipticals may be due to the fact that they have injected most of their metals to the intracluster gas rather than recycling the material for their own stars. The opposite would then be true for dwarf ellipticals in the outer cluster regions, their metallicities are enhanced relative to the core because they have held onto their metal enriched gas for later generations. Thus, the intracluster gas was deprived of their metals and have lower [Fe/H] values in the halo, resulting in a decreasing ICM abundance gradient with cluster radius. The mechanism for this process is, presumingly, ram-pressure gas stripping by the intracluster medium and this process should be more effective on low-mass objects, such as dwarf ellipticals, than high-mass galaxies because of their shallower gravitational potentials.

An addition test to the clusters influence is to examine the mean ages of the dE's as a function of cluster radius. If the outer dwarfs have higher metallicities due to a delay in stripping by the cluster ICM, then we would expect to find a younger mean age reflecting the longer duration of star formation and continued metal processing. Likewise, for the inner galaxies, we would expect to find an older mean age reflecting the earlier shutdown of star formation by the ICM. In fact, the distribution of ages indicates that this is the case. Figure 14 plots dE's with greater than or less than 10 Gyr ages based on the $\Delta(bz-yz)$ index. As expected, a majority of the dE's within a radius of 0.7 Mpc are older than 10 Gyr. This would also explain why Trager et al. (2000) find a range of elliptical ages in the field, but Kuntschner (2000) find only old, coeval ellipticals in the Fornax cluster. The cluster environment appears to play a major role in the cession of initial star formation in ellipticals much like the cluster environment effects infalling spirals at intermediate redshifts (i.e., the Butcher-Oemler effect).

4. CONCLUSIONS

The first part of this paper was spent examining the behavior of our narrowband filter system under changes in age and metallicity using globular cluster data and SSP models. The calibrations and multimetallicity population models produce excellent fits to the past data on both bright and dwarf ellipticals. Using these calibrations, we present a new set of narrowband photometry for Fornax dwarf ellipticals. We can summarize our results as the following:

1. The dwarf ellipticals in Fornax are found to have [Fe/H] values ranging from -1.6 to -0.4 with a mean of -1.0. The ages of dwarfs ellipticals have a mean of 10 ± 1 Gyr. For comparison, the color-magnitude relation for bright ellipticals ($M_B < -18$) converts into a range of [Fe/H] from -0.5 at the faint end to $+0.3$ for the most massive systems, in agreement with previous studies. These values are based on luminosity-weighted colors corrected by our multimetallicity models. The $\Delta(bz-yz)$ index indicates that the bright ellipticals in clusters have a mean age of 13 Gyr, on average 3 Gyr older than dwarfs, with very little scatter (i.e., coeval, see Kuntschner 2000).

2. The [Mg/Fe] ratio reflects the abundance of α elements to Fe which varies due to the relative contribution from Type Ia and Type II SNe. The data for dwarf ellipticals indicate [Mg/Fe] values slightly higher than Galactic globular cluster, but near solar. The $vz-yz$, Mg_2 relationship for bright ellipticals indicates a trend of increasing [α/Fe] with mass.

3. The Fornax dwarf ellipticals do not, as a group, follow a mass-metallicity relation found for bright ellipticals. However, there is good evidence to indicate that the dwarfs divide into high- and low-metallicity sequences based on mean age. The younger dwarfs have higher metallicities per mass, which suggests a longer or more intensive period of star formation and resulting chemical evolution before the onset of galactic winds.

4. There is a clear abundance and age gradient for Fornax dwarfs within the cluster environment. The gradients are such that older, metal-poor dwarfs inhabit the central core of the cluster and the younger, metal-richer dwarfs occupy the halo.

As pointed out in Trager et al. (2000), there are numerous scenarios that can lead to either an increasing [Fe/H] or an increasing [α/Fe] with galaxy mass. However, it is difficult to resolve both effects with either a simple increase in the initial star formation duration, or with earlier and stronger galactic winds for low-mass systems. With respect to the Fornax dwarfs, a somewhat clear picture presents itself because of the fact that the older dwarfs have higher metallicities and the [α/Fe] values for dwarfs in general are near solar. This suggests that star formation in dwarf ellipticals occurs in a long, weak initial burst, sufficiently long to acquire low [α/Fe] values from Type Ia SN enrichment, but also sufficiently low in strength to inhibit the onset of a galactic wind. Any extrapolation of this style of star formation to bright ellipticals requires that the duration of initial star formation decrease with increasing galaxy mass, which reconciles the increasing [α/Fe] ratio with mass. But, the strength of the burst must also increase with galaxy mass to increase the number of stellar generations in order to reconcile the increase in [Fe/H] with galaxy mass. A stronger burst will inject more energy at a higher rate and, thus, produce an earlier galactic wind.

The remaining mystery for the chemical evolution of dwarf ellipticals is the extremely large spread in [Fe/H] values per mass bin. If star formation in dwarfs is halted by a galactic wind, then the mass metallicity relation should continue into the dwarf regime. However, the galactic wind idea for dwarfs has come into question by Mac Low & Ferrara (1999) who propose, based on analytic and numerical simulations, that galactic winds in dwarfs are impossible for masses above $10^9\ M_\odot$. Their model is primarily motivated by the concept that the hot gas within the SN superbubble is easily heated to escape velocity, but the surrounding cold gas must also be sweep up and accelerated, a much more difficult energy requirement. Without a galactic wind, star formation duration would seem to be the controlling factor in determining the final metallicity of a dwarf galaxy. And this is confirmed in Figure 13, such that the dwarfs with the longest epoch of star formation have the highest metallicities.

Lastly, the information culled from Figure 14 suggests a strong environmental influence on the star formation history of dwarf ellipticals. While it has been proposed that dwarf galaxies may contribute some fraction of the ICM in rich clusters (Nath & Chiba 1995; Trentham 1994), there is no direct evidence that metal enriched gas has been removed from cluster dwarf galaxies. Without interpretation, the correlation of metallicity and age indicates that star formation is halted by some mechanism, prematurely, for core galaxies (old age) which, in turn, ceases chemical

evolution (lower metallicities). The most likely candidate for this mechanism is ram-pressure stripping (Gunn & Gott 1972); however, alternative scenarios, such as galaxy harassment (Moore et al. 1996), have been proposed (see Skillman & Bender 1995 for a review). Further observations into the spread of metallicity and age within a cluster and addition knowledge of the range of [α/Fe] among cluster dwarfs will be required to better define the problem.

The authors wish to thank the directors and staff of CTIO and Steward and Lowell observatories for granting time for this project. Financial support from Austrian Fonds zur Foerderung der Wissenschaftlichen Forschung is gratefully acknowledged. We also wish to thank the referee, Scott Trager, for his numerous suggestions and comments that strengthened the presentation of our data.

REFERENCES

Alcaino, G., Liller, W., & Alvarado, F. 1997, AJ, 114, 2626
Arimoto, N. 1996, in ASP Conf. Ser. 98, From Stars to Galaxies: The Impact of Stellar Physics on Galaxy Evolution, ed. C. Leitherer, U. Fritze-von Alvensleben, & J. P. Huchra (San Francisco: ASP), 287
Arimoto, N., & Yoshii, Y. 1987, A&A, 173, 23
Arnaud, M., Rothenflug, R., Boulade, O., Vigroux, L., & Vangioni-Flam, E. 1992, A&A, 254, 49
Bothun, G., & Mould, J. 1988, ApJ, 324, 123
Bothun, G., Mould, J., Caldwell, N., & MacGillivray, H. 1986, AJ, 92, 1007
Bower, R., Lucey, J., & Ellis, R. 1992, MNRAS, 254, 589
Bressan, A., Chiosi, C., & Tantalo, R. 1996, A&A, 311, 425
Brodie, J., & Huchra, J. 1991, ApJ, 379, 157
Bruzual, A., & Charlot, S. 2001, in preparation (BC2001)
Buonanno, R., Corsi, C., Castellani, M., Marconi, G., Fusi Pecci, F., & Zinn, R. 1999, AJ, 118, 1671
Caldwell, N., Armandroff, T., Da Costa, G., & Seitzer, P. 1998, AJ, 115, 535
Caldwell, C., & Bothun, G. 1987, AJ, 94, 1126
Carretta, E., & Gratton, R. 1997, A&AS, 121, 95
Carretta, E., Gratton, R., Clementini, G., & Fusi Pecci, F. 2000, ApJ, 533, 215
Cellone, S., & Forte, J. 1996, ApJ, 461, 176
Charlot, S., & Bruzual, G. 1991, ApJ, 367, 126
da Costa, G. 1998, in Stellar Astrophysics for the Local Group, ed. A. Aparicio, A. Herrero, & F. Sanchez (Cambridge: Cambridge Univ. Press), 351
Dupke, R. & White, R. 2000, ApJ, 537, 123
Elmegreen, B., et al. 2000, AJ, 120, 630
Fiala, N., Rakos, K., & Stockton, A. 1986, PASP, 98, 70
Ferguson, H. 1989, AJ, 98, 367
Ferguson, H., & Binggeli, B. 1994, A&A Rev., 6, 67
Geisler, D., & Forte, J. 1990, ApJ, 350, L5
Gibson, B., & Matteucci, F. 1997, ApJ, 475, 47
Greggio, L. 1997, MNRAS, 285, 151
Guiderdoni, B., & Rocca-Volmerange, B. 1987, A&A, 186, 1
Gunn, J., & Gott, R. 1972, ApJ, 176, 1
Hanes, D., & Harris, W. 1986, ApJ, 309, 564
Harris, W. 1996, AJ, 112, 1487
Held, E., & Mould, J. 1994, AJ, 107, 1307
Ishimaru, Y., & Arimoto, N. 1997, PASJ, 49, 1
Kodama, T., & Arimoto, N. 1997, A&A, 320, 41
Kobayashi, C., Tsujimoto, T., Nomoto, K., & Hachisu, I. 1998, ApJ, 503, L155
Kronawitter, A., Saglia, R., Gerhard, O., & Bender, R. 2000, A&AS, 144, 53
Kuntschner, H. 2000, MNRAS, 315, 184
Kuntschner, H., Lucey, J., Smith, R., Hudson, M., & Davies, R. 2000, MNRAS, in press
Larson, R. 1974, MNRAS, 166, 585
Lee, Y., Demarque, P., & Zinn, R. 1994, ApJ, 423, 248
Liu, M., Graham, J. & Charlot, S. 2000, ASP Conf. Ser. 201, Cosmic Flows 1999: Toward and Understanding of Large-Scale Structures, ed. S. Courteau, M. A. Strauss, & J. A. Willick (San Francisco: ASP), 142
Mac Low, M., & Ferrara, A. 1999, ApJ, 513, 142
Madore, B., et al. 1999, ApJ, 515, 29
Matteucci, F. 1992, ApJ, 397, 32
Moore, B., Katz, N., Lake, G., Dressler, A., & Oemler, A. 1996, Nature, 379, 613
Mould, J. 1984, PASP, 96, 773
Nath, B., & Chiba, M. 1995, ApJ, 454, 604
O'Neil, K., Bothun, G., Smith, E., & Stecher, T. 1996, AJ, 112, 431
Peterson, R., & Caldwell, N. 1993, AJ, 105, 1411
Prugniel, P., Bica, E., Klotz, A., & Alloin, D. 1993, A&AS, 99, 229
Rakos, K., Fiala, N., & Schombert, J. 1988, ApJ, 328, 463
Rakos, K., Maindl, T., & Schombert, J. 1996, ApJ, 466, 122
Rakos, K., & Schombert, J. 1995, ApJ, 439, 47
Rakos, K., Schombert, J., Odell, A., & Steindling, S. 2000, ApJ, 540, 715
Rutledge, G., Hesser, J., & Stetson, P. 1997, PASP, 109, 907
Salaris, M., & Weiss, A. 1998, A&A, 335, 943
Salasnich, B., Girardi, L., Weiss, A., & Chiosi, C. 2000, A&A, 361, 1023
Sandage, A., Binggeli, B., & Tammann, G. 1985, AJ, 90, 1759
Schombert, J., Hanlan, P., Barsony, M., & Rakos, K. 1993, AJ, 106, 923
Skillman, E., & Bender, R. 1995, in Rev. Mexicana Astron. Astrofis. 3, Gaseous Nebulae and Star Formation, ed. M. Peña & S. Kurtz (México, D.F.: Inst. Astron.), 25
Stetson, P., et al. 1999, AJ, 117, 247
Stetson, P., Vandenberg, D. & Bolte, M. 1996, PASP, 108, 560
Strömgren, B. 1966, ARA&A, 4, 433
Tantalo, R., Chiosi, C., & Bressan, A. 1998, A&A, 333, 419
Tantalo, R., Chiosi, C., Bressan, A., & Fagotto, F. 1996, A&A, 311, 361
Terlevich, R., Davies, R., Faber, S., & Burstein, D. 1981, MNRAS, 196, 381
Thuan, T. 1985, ApJ, 299, 881
Trager, S., Faber, S., Worthey, G., & Gonzalez, J. 2000, AJ, 120, 165
Trentham, N. 1994, Nature, 372, 157
Weiss, A., Peletier, R., & Matteucci, F. 1995, A&A, 296, 73
Wheeler, J., Sneden, C. & Truran, J. 1989, ARA&A, 27, 279
Wood, D. B. 1969, AJ, 74, 177
Worthey, G. 1994, ApJS, 95, 107
———. 1998, PASP, 110, 888
Worthey, G., Dorman, B., & Jones, L. 1996, AJ, 112, 948
Worthey, G., Faber, S., & Gonzalez, J. 1992, ApJ, 398, 69
Yoshii, Y., & Arimoto, N. 1987, A&A, 188, 13
Zinn, R. 1985, ApJ, 293, 424